



**HAL**  
open science

**Geochemical evidence for carbon and chlorine enrichments in the mantle source of kimberlites (Udachnaya pipe, Siberian craton)**

Yumi Kitayama, Emilie Thomassot, Albert Galy, Andrey Korsakov, Alexander Golovin, Elisabeth d'Eyramés

► **To cite this version:**

Yumi Kitayama, Emilie Thomassot, Albert Galy, Andrey Korsakov, Alexander Golovin, et al.. Geochemical evidence for carbon and chlorine enrichments in the mantle source of kimberlites (Udachnaya pipe, Siberian craton). *Geochimica et Cosmochimica Acta*, 2021, 315, pp.295-316. 10.1016/j.gca.2021.09.021 . hal-03800806

**HAL Id: hal-03800806**

**<https://hal.science/hal-03800806v1>**

Submitted on 5 Jan 2024

**HAL** is a multi-disciplinary open access archive for the deposit and dissemination of scientific research documents, whether they are published or not. The documents may come from teaching and research institutions in France or abroad, or from public or private research centers.

L'archive ouverte pluridisciplinaire **HAL**, est destinée au dépôt et à la diffusion de documents scientifiques de niveau recherche, publiés ou non, émanant des établissements d'enseignement et de recherche français ou étrangers, des laboratoires publics ou privés.



Distributed under a Creative Commons Attribution - NonCommercial 4.0 International License

1 **Geochemical evidence for carbon and chlorine enrichments in the mantle**  
2 **source of kimberlites (Udachnaya, Siberia)**

3  
4

5 **Authors**

6 Yumi Kitayama<sup>1</sup>, Emilie Thomassot<sup>1\*</sup>, Albert Galy<sup>1</sup>, Andrey Korsakov<sup>2</sup>, Alexander Golovin  
7 <sup>2,3</sup>, Elisabeth d'Eyrames<sup>1</sup>

8

9 1 Université de Lorraine, Centre de Recherches Pétrographiques et Géochimiques, CNRS, 15  
10 Rue Notre Dame des Pauvres, BP 20, 54 501 Vandœuvre-lès-Nancy, France.

11 2 Sobolev Institute of Geology and Mineralogy, Siberian Branch, Russian Academy of  
12 Science, Prosp. Ak. Koptiyuga 3, 630090 Novosibirsk, Russian Federation

13 3 Institute of the Earth's Crust, Siberian Branch of the Russian Academy of Sciences,  
14 Lermontov Street 128, Irkutsk 664033, Russian Federation

15 \* Corresponding author: Emilie Thomassot ([emilie.thomassot@univ-lorraine.fr](mailto:emilie.thomassot@univ-lorraine.fr)).

16

17 **Keywords: kimberlite, salts, alkali-carbonate, sulfate, lithospheric mantle, Siberian**  
18 **craton, chloride carbonate liquid segregation**

19

20 **Abstract**

21

22 Deep, carbonate-rich melts are key constituents of kimberlites and are crucial for  
23 understanding the cycle of volatile elements in the mantle. On the Siberian craton, the  
24 Udachnaya-East kimberlite hosts extremely well-preserved nodules composed of chlorides +  
25 carbonates + sulfates, that do not present any relict sedimentary textures. These salty nodules  
26 display textures that are commonly observed in quenched liquids and may thus represent the  
27 very last stage liquid of the kimberlite. Alternatively, they could represent assimilated  
28 sedimentary material, or even post-magmatic hydrothermal alteration, because kimberlites are  
29 known to ascend through the lithosphere while assimilating material from their wall rocks.

30 Here we focus specifically on those chloride-carbonate nodules, which are composed  
31 of 70% chloride + 30% alkali-carbonate and sulfate, and used two radiogenic systems (Rb-Sr,  
32 Sm-Nd) and the isotopic composition of sulfur, in addition to their major and trace element  
33 compositions (n=3). We then compared the results with the same geochemical data on host  
34 kimberlites (n=4), sedimentary cover (n=3) and hydrothermal veins (n=3).

35 Taken together, our results show that the nodules are not the product of a  
36 contamination by the Cambrian sedimentary cover. Trace element patterns of the nodules  
37 display extreme enrichments in the same elements that are relatively depleted in the host  
38 kimberlite but also in kimberlites worldwide (K, Rb, Sr, Pb), suggesting that chloride-  
39 carbonate nodules are snapshots of the latest stage liquid present in the kimberlite system.  
40 Their isotopic compositions (Rb-Sr, Sm-Nd and  $\delta^{34}\text{S}$ ) are consistent with a common  
41 magmatic source with their host kimberlite. We propose that chloride-carbonate nodules  
42 record a missing compositional endmember, which could explain the trend towards more  
43 radiogenic Sr isotope ratios at nearly constant Nd signatures observed in their host kimberlite,  
44 as well as in other kimberlites worldwide. This observed trend suggests the presence of a  
45 recycled component with high Rb/Sr (such as salts or terrigenous sediments) in the mantle  
46 sampled by some kimberlites, either in the lithosphere or the asthenosphere. This study  
47 highlights that the role of alkalis and halogens may have been underestimated in the genesis  
48 of kimberlites at depths where diamonds are stable, as well as in more evolved magmatic  
49 stages. Segregations of chlorides and carbonates occur specifically in sulfate-bearing  
50 kimberlites, which may thus sample a mantle domain in which sulfates with  $\delta^{34}\text{S} > 0\text{‰}$  are  
51 dominant. The existence of such a reservoir could explain the apparent imbalance observed  
52 between the chondritic value ( $\delta^{34}\text{S}$  of 0‰) and the negative S isotopic compositions of mantle  
53 sulfides (MORB and peridotites).

## 54 **1. Introduction**

55

56 Kimberlites are volatile-rich volcanic rocks of alkaline composition that contain abundant  
57 olivine crystals. Their parental magma originates at great depth beneath continents, in the  
58 diamond stability field (>150 km depth). Although the exact nature of their parental magma  
59 does not reach a consensus yet, there is evidence for the participation of halogens and other  
60 volatiles as well as alkaline elements in the genesis of kimberlites. Some key observations  
61 include the presence of syngenetic phlogopite inclusion in kimberlite-hosted diamonds with  
62 up to 0.5 wt% Cl (Sobolev et al., 2009), Na ± K-rich compositions of residual melts/fluids (C-  
63 O-H-Cl bearing) after olivine crystallization (Golovin et al., 2007; Kamenetsky et al., 2009,  
64 2014; Giuliani et al., 2017; Abersteiner et al., 2018), as well as Na ± K-chloride inclusions in  
65 chromite, perovskite, apatite (Abersteiner et al., 2017), magmatic calcite and olivine from  
66 Udachnaya (Tomilenko et al., 2017a, b).

67 The presence of salts at depth raises the exciting question of volatile recycling through  
68 time, and its ultimate role on mantle metasomatism, especially upon the compositional  
69 spectrum of mantle fluids (Izraeli et al., 2001; Klein-BenDavid et al., 2007; Weiss et al.,  
70 2015; Zedgenizov et al., 2018). However, the primary origin and concentration of chlorine  
71 and other volatiles in various kimberlites worldwide is difficult to unravel because: (1)  
72 volatiles are often lost via exsolution during ascent and emplacement, as well as post-  
73 emplacement alteration (Abersteiner et al., 2017); (2) each kimberlite composition reflects  
74 some assimilation of the local lithospheric mantle directly underneath (Francis and Patterson,  
75 2009; Tappe et al., 2011; Giuliani et al., 2020), and (3) the percolation of late stage fluids as  
76 well as the assimilation of sedimentary or crustal xenoliths during magma ascent near the  
77 surface (Kjarsgaard et al., 2009), can seriously modify the primary composition of  
78 kimberlites.

79 On the Siberian craton, the Udachnaya-East kimberlite preserves a rare, dry (H<sub>2</sub>O <0.5  
80 wt%) and serpentine-free rock type with anomalously high contents of chlorine (up to 6.1  
81 wt%), alkalis (Na<sub>2</sub>O+K<sub>2</sub>O up to 10 wt%) and sulfur (S up to 0.50 wt%), referred to as a  
82 “salty” kimberlite (Kamenetsky et al., 2012; D’Eyrames et al., 2017). This salty kimberlite  
83 contains nodules composed of carbonate, chloride and sulfate, whose origin is a matter of  
84 debate and could be either: (1) the segregation by immiscibility from a liquid initially derived  
85 from melting of the mantle (Maas et al., 2005; Kamenetsky et al., 2007, 2014), (2) the  
86 assimilation of sediments or crustal xenoliths by the ascending magma (Kopylova et al.,  
87 2013), or (3) a post-magmatic hydrothermal alteration (Kopylova et al., 2013). According to

88 sulfur isotopic compositions, abundant sulfates found in the salty kimberlite of Udachnaya-  
89 East derive from an oxidized, sulfate-bearing mantle source (Kitayama et al., 2017). Such  
90 mantle domains, if confirmed, would represent a little explored but significant reservoir in the  
91 global geochemical cycle of volatile elements.

92 In this study, we investigated the genetic link between the chloride-carbonate nodules  
93 and their host kimberlite, as well as their possible sources (asthenosphere, lithosphere,  
94 granitic crust or sediments). For this purpose, we used a combination of two radiogenic  
95 systems (Rb-Sr, Sm-Nd) and the stable isotopic composition of sulfur in chloride-carbonate  
96 nodule, salty kimberlite, as well as hydrothermal salts, sulfates, a regional brine and the only  
97 salt-bearing host sediment found in drill holes in the area. Our results exclude the Cambrian  
98 sedimentary cover as a source of chloride-carbonate nodules and instead support a mantle  
99 origin. Calculations of age-corrected  $^{87}\text{Sr}/^{86}\text{Sr}$  and  $^{143}\text{Nd}/^{144}\text{Nd}$  ratios as well as S isotopes  
100 allowed us to evaluate possible scenarios for the source of salts in nodules and kimberlites.

101

102

103

## 104 **2. Geological setting**

105

106 The Udachnaya-East kimberlite is located in the Daldyn kimberlite field (Aldan province) in  
107 the central part of the Siberian craton (Fig. 1). At the craton scale, several kimberlite  
108 emplacements from early Devonian to late Jurassic have been reported (Sun et al., 2014). In  
109 the Aldan province however kimberlite emplacement ages mostly range from 340 to 360 Ma,  
110 with minor occurrences in the intervals 420–400 and 600–500 Ma. The oldest recorded ages  
111 (600–500 Ma) may represent older mantle material within the bulk kimberlites, rather than the  
112 actual ages of kimberlite activities (Smelov and Zaitsev, 2013). The Udachnaya-East  
113 kimberlite was emplaced ~365 Ma, as indicated by  $^{40}\text{Ar}$ – $^{39}\text{Ar}$  ( $362.7\pm 3.7$  Ma) and Rb–Sr  
114 cooling ages ( $364.6\pm 4.1$  Ma) from phlogopite in a kimberlitic clast (Kamenetsky et al., 2009)  
115 and U–Pb age ( $367\pm 5$  Ma) of perovskite from the host Udachnaya-East kimberlite (Kinny et  
116 al., 1997).

117 The Udachnaya-East kimberlite was emplaced in a sedimentary sequence ranging in  
118 thickness from 2500 m in the northeast to 3100 m in its southwestern part (Kamenetsky et al.,  
119 2014 and references therein) and covering a basement of Archean-Proterozoic crustal rocks  
120 (Smelov and Zaitsev, 2013). The ages of the sedimentary cover range from early to late  
121 Cambrian (542 to 488 Ma). Massive salt beds of the Cambrian evaporite cover are present

122 ~400 km south of Udachnaya around the MIR and International'naya kimberlite pipes (Fig.  
123 1), but are absent in sediments in the vicinity of Udachnaya (Kamenetsky et al., 2014 and  
124 references therein). At Udachnaya, sediments consist mainly of shales, dolomites, marls, and  
125 limestones. Dolomites of the Chukuck suite are the only host rock that contain sulfate-rich  
126 veins (Fig. 2-e) and may also contain salts, although these veins are only present locally.  
127 These sulfate veins could represent a Cambrian analogue of sabkha where evaporites and  
128 dolomites are mixed or alternatively they could have precipitated hydrothermally from brines  
129 (Kamenetsky et al., 2014; Kopylova et al., 2016). Indeed, Udachnaya is located within an area  
130 of modern brines (Fig. 1), and the precipitation of halite from saline groundwaters (300 g/l)  
131 has been observed in the open-pit mine (Kopylova et al., 2013 and references therein). The  
132 presence of a Vendian carbonate and evaporite belt with sedimentological characteristics  
133 similar to the Chukuck suite were expected just above the crystalline basement (Kopylova et  
134 al., 2013 and references therein) but could not be verified, despite extensive drilling near the  
135 Udachnaya-East pipe (Kamenetsky et al., 2014).

136

137

### 138 **3. Sample description**

139

140 Chloride-carbonate nodules were collected from stockpiles of salty kimberlite mined from  
141 460-500 m depths. They are rounded or angular, range in size from 3 to 10 cm, and consist of  
142 30 to 70% of carbonate, the remaining part being chlorides (Table 1). They do not present any  
143 relic sedimentary textures, indicating that they were completely molten before they  
144 crystallized in the kimberlite. The samples present intergrowths of randomly oriented sheets  
145 of chloride and carbonates (Fig. 2-a and b). These textures are reminiscent of immiscibility  
146 between alkaline-carbonate and alkaline-chloride liquids observed ~600°C in melt inclusions  
147 trapped in olivine from the same kimberlite (Kamenetsky et al., 2007). Chlorides in these  
148 nodules are transparent, greyish (Fig. 2-a and -b) and consist of massive halite (NaCl) with  
149 sylvite (KCl) globules (Kamenetsky et al., 2007). Carbonates are opaque, white (Fig. 2-a and  
150 -b) and display a wide range of alkaline-carbonate compositions ( $\text{Na-Ca} \pm \text{K} \pm \text{S}$ ), showing a  
151 positive correlation between  $\text{SO}_3$  (up to 13 wt%) and  $\text{K}_2\text{O}$  contents (up to 14 wt%;  
152 Kamenetsky et al., 2007). Among these alkali-carbonates, shortite ( $\text{Na}_2\text{Ca}_2(\text{CO}_3)_3$ ) and  
153 northupite ( $\text{Na}_3\text{Mg}(\text{CO}_3)_2\text{Cl}$ ) have previously been identified in similar samples (Kamenetsky  
154 et al., 2007). Raman spectra of shortite from a chloride-carbonate nodule also show the  
155 presence of  $\text{SO}_4$  groups which are either incorporated in the carbonate structure (replacing

156 some CO<sub>3</sub> groups) or form very fine exsolution lamellae of aphtitalite ((K,Na)<sub>3</sub>Na(SO<sub>4</sub>)<sub>2</sub>;  
157 D'Eyrames et al., 2017). Finally, most sulfide were too small to be identify in hand specimen  
158 and impossible to prepare in thin section due to the nature of the samples. Only one galena  
159 crystal (PbS) and one djerfisherite crystal (K<sub>6.05</sub>Na<sub>0.6</sub>(Fe<sub>19.27</sub>Ni<sub>0.47</sub>Cu<sub>3.53</sub>)S<sub>26</sub>Cl<sub>0.91</sub>) have been  
160 characterized.

161 To relate these nodules to kimberlite magmatism, we studied four samples of the host  
162 kimberlite, carefully chosen with minimal signs of alteration or contamination. Three samples  
163 have crustal contamination indices (C.I.) < 1 (Table 2, C.I. = (SiO<sub>2</sub> + Al<sub>2</sub>O<sub>3</sub> + Na<sub>2</sub>O) / (MgO  
164 + 2\*K<sub>2</sub>O), Kjarsgaard et al., 2009), indicating little crustal contamination. Only one sample  
165 (UV12-119) had C.I. = 1.6. Although this index is not relevant for quantifying the  
166 contamination by surficial lithology (e.g. sediments), it gives an indication of the possible  
167 incorporation of continental granitic crust. For an accurate comparison with possible sources  
168 of contamination and post-magmatic alteration, we analyzed hydrothermal veins (Fig. 2-c and  
169 -d), a sample of country-rock dolomite containing a sulfate-bearing vein (n=1; Fig. 2-e), a  
170 sample of regional brine (n=1; Fig. 2-g) and brine precipitates (n=1; Fig. 2-f). The brine  
171 sample contains sulfates and was collected from a depth of 750 m in a drill hole 1 km south of  
172 Udachnaya. Brine precipitates were collected from 520 m depth in the open pit itself, where  
173 they had crystallized after the evaporation of brines from host sediments. The sample of host  
174 sediment (dolomite of the Chukuck suite, UV09-305 Fig. 2-e) represents the only known  
175 portion of crustal material that may provide sulfate- and perhaps salt-rich xenoliths to the  
176 kimberlite. It was collected at a depth of 630 m in a drill hole located between the West and  
177 East kimberlite bodies of Udachnaya.

## 178 **4. Analytical techniques**

179

### 180 **4.1. Whole rock major and trace element analyses**

181

182 Pieces of chloride-carbonate nodules were selected from the interior of the nodules, to avoid  
183 contamination by the surrounding kimberlite groundmass. Samples from hydrothermal veins  
184 were also selected free of kimberlitic material. Samples of rock powders and brine were  
185 analysed for major and trace element geochemistry by the SARM laboratory (Service  
186 d'Analyses des Roches et des Minéraux, Vandœuvre-Les-Nancy, France). Major element  
187 analyses were carried out using an inductively coupled-plasma optical emission spectrometer  
188 (ICP OES Icap 6500, from ThermoFisher) and trace element compositions were measured  
189 using an inductively coupled-plasma mass-spectrometer (ICP-MS iCapQ from  
190 ThermoFisher). Chlorine concentrations were measured by ultraviolet-visible  
191 spectrophotometry / potentiometric titration. For whole rock analyses, total CO<sub>2</sub> and S were  
192 measured using an elemental analyser while H<sub>2</sub>O+ (referring to water within mineral  
193 structures) was measured by Karl-Fisher titration. Major element compositions are expressed  
194 both in atomic wt.% and oxide wt.% (Table 2), because oxide wt.% is not applicable for  
195 chlorides analyses (NaCl, KCl) and can lead to erroneous totals (<100 wt.% when Cl  
196 concentrations are not included and >100 wt.% when included). Trace element compositions  
197 are expressed in ppm (Table 3). For the brine solution, measured concentrations were  
198 normalized to 100% to enable for a comparison with rock samples.

199

### 200 **4.2. Radiogenic isotopes**

201

#### 202 ***Sequential chemical leaching***

203 Whole rock analyses were applied on 200 mg porphyzied powder for samples of  
204 chloride-carbonate nodules, 300 mg for samples of salty kimberlites and 500 mg for the host  
205 sediment. Powdered samples were digested according to a method of sequential leaching in  
206 order to avoid the formation of fluorides. A series of chemical leaching separated the water-  
207 soluble (mainly chlorides), acid-soluble (mainly carbonate) and residual fractions (mainly  
208 silicates) of powdered samples. In order to dissolve the water-soluble phases, we started with  
209 leaching the samples twice in de-ionized water (18.2 MΩ.cm) at room temperature. This was  
210 followed by leaching twice in acetic acid (10 vol. %) in order to dissolve the acid-soluble  
211 phases. Before and after each leaching step of this procedure, we estimated the proportions of

212 leached material by drying and weighing the solid residue. The silicate residue was then  
213 digested using hydrofluoric and nitric acids, following the procedure described in Alibert et  
214 al. (1983) and Michard et al. (1985). During the preparation of the silicate residue of the host  
215 sediment sample, fluorides precipitated. For this sample, we thus only dissolved and analysed  
216 the leachate (Table 1). For all other samples (chloride-carbonate nodules and salty  
217 kimberlites), we then mixed the three isolated fractions in order to obtain material  
218 representative of whole rock samples.

219 We then separated the sample solutions in separate aliquots for Sr, Rb and Sm-Nd  
220 analyses. Next, we spiked the aliquots with tracers of  $^{85}\text{Rb}$ ,  $^{84}\text{Sr}$  and mixed  $^{149}\text{Sm}$ - $^{150}\text{Nd}$   
221 respectively. We equilibrated the spike and sample for more than 24 hours before separating  
222 rare earth elements (REEs), Rb, Sr, Sm and Nd by column chromatography. REEs were  
223 separated first using TRU-spec resin (Pin et al., 1994). For samples of chloride-carbonate  
224 nodules and host sediment, Rb and Sr were then separated using AG50-X8 cation resin (e.g.  
225 Alibert et al. 1983). For samples of salty kimberlites, Rb and Sr were separated using Sr-spec  
226 resin (Horwitz et al., 1992). Finally, in both cases, Sm and Nd were separated using LN-spec  
227 resin (Pin et al., 1997).

228

### 229 *Rb-Sr isotope analyses*

230 Rb concentrations were determined by isotopic dilution, measuring the isotopic  
231 composition of spiked samples on an ICPMS Quadrupole (ThermoScientific X-Series 2). To  
232 avoid bias related to the interference of  $^{87}\text{Sr}$  on  $^{87}\text{Rb}$ , we always monitored the signal of  $^{88}\text{Sr}$ .  
233 When the Rb was not sufficiently purified of Sr (e.g., in samples with extremely high Sr  
234 concentration), we did not use the Rb concentrations obtained from the spiked samples. Sr  
235 concentrations and isotopic compositions ( $^{86}\text{Sr}$ ,  $^{87}\text{Sr}$ ,  $^{88}\text{Sr}$ ,  $^{84}\text{Sr}$ ) of spiked samples were  
236 determined on TIMS (Thermal Ionization Mass Spectrometry - ThermoScientific Triton).  
237 Mass-dependent fractionation was corrected to a  $^{86}\text{Sr}/^{88}\text{Sr}$  ratio of 0.1194 by the exponential  
238 law and  $^{87}\text{Sr}/^{86}\text{Sr}$  ratio of the NBS987 was  $0.710248 \pm 0.000025$  ( $2\sigma$ ,  $n = 10$ ) during the  
239 course of the analyses.

240 By mass, total analytical blanks represented  $\leq 0.0003\%$  of the Rb and  $\leq 0.01\%$  of the  
241 Sr contained in the water leachates; they represented  $\leq 0.004\%$  of the Rb and  $\leq 0.0002\%$  of  
242 the Sr contained in the acetic acid leachates; and  $\leq 0.003\%$  of the Rb and 0.0015 to 0.3% of  
243 the Sr contained in whole-rock material.  $^{87}\text{Sr}/^{86}\text{Sr}$  isotopic compositions of the blank were  
244  $0.703 \pm 0.003$  ( $2\sigma$ ) for water leachates,  $0.7090 \pm 0.0003$  for acid leachates and  $0.7081 \pm$   
245  $0.0007$  for whole-rock material. Isotopic compositions of blanks are variable but uncorrelated

246 to Rb and Sr concentrations. Rb-Sr data presented in Table 4 are corrected for blank  
247 contribution. Reported uncertainties at the  $2\sigma$  level correspond to error propagation of  
248 individual measurements and blank correction. The analytical precision of concentrations  
249 determined by isotopic dilution are  $\sim 0.5\%$  for Rb and  $\sim 0.2\%$  for Sr. Uncertainties on  
250  $^{87}\text{Rb}/^{86}\text{Sr}$  ratios are better than  $0.1\%$  for ratios  $> 1$ . For whole-rock kimberlite samples, Rb  
251 concentrations could not be determined by isotopic dilution (incomplete purification of Rb  
252 fractions), so we used the concentrations measured by ICP-MS at the SARM laboratory, with  
253 larger uncertainties of  $5\%$  (Table 4). Uncertainties on the low  $^{87}\text{Rb}/^{86}\text{Sr}$  ratios of these  
254 samples thus appear to be significantly larger as well (10 to  $25\%$  of the values), but are highly  
255 overestimated.

256

### 257 *Sm-Nd isotope analyses*

258 Concentrations of Sm and Nd were measured by isotopic dilution using a mixed Sm-  
259 Nd spike and measuring Sm ( $^{146}\text{Nd}$ ,  $^{147}\text{Sm}$ ,  $^{149}\text{Sm}$ ,  $^{155}\text{Gd}$ ,  $^{148}\text{Sm}$ ) and Nd isotopic  
260 compositions ( $^{143}\text{Nd}$ ,  $^{146}\text{Nd}$ ,  $^{147}\text{Sm}$ ,  $^{142}\text{Nd}$ ,  $^{144}\text{Nd}$ ,  $^{145}\text{Nd}$ ) during two separate sessions on a  
261 MC-ICP MS (multi-collector inductively coupled plasma mass spectrometer - Neptune Plus).  
262 For Nd isotope measurements, the instrument was equipped with an Apex HF desolvating  
263 nebulizer (ESI) for increased sensitivity.  $^{143}\text{Nd}/^{144}\text{Nd}$  ratios were first normalised to  
264  $^{146}\text{Nd}/^{144}\text{Nd} = 0.7219$  using an exponential law and then to the JNdi-1 following a pseudo (1  
265 standard each 4-5 samples) standard-sample bracketing method (Yang et al., 2017).

266 Total analytical uncertainty represented  $4.8$  to  $5.6\%$  of the Sm mass and  $1.2$  to  $1.3\%$   
267 of the Nd mass contained in whole-rock material.  $^{143}\text{Nd}/^{144}\text{Nd}$  isotopic compositions of the  
268 blank was  $0.512231 \pm 0.000577$  ( $2\sigma$ ) for water leachates,  $0.511551 \pm 0.000620$  for acetic acid  
269 leachates and  $0.512137 \pm 0.000578$  for whole-rock material. Blanks levels are high and  
270 characterized by variable isotopic compositions, which suggests that blanks are related to both  
271 the long evaporation times resulting from handling large amounts of samples, and to the  
272 complex procedure of subsequent leachings and recombining of solutions (designed to avoid  
273 the formation of fluoride). Whole rock compositions for Sm and Nd are reported after  
274 correcting for blank contribution (Table 5). Reported uncertainties at the  $2\sigma$  level correspond  
275 to error propagation of individual measurements and blank correction. Precisions on Sm and  
276 Nd concentrations were always better than  $0.2\%$  for both Sm and Nd. Whole-rock  
277  $^{147}\text{Sm}/^{144}\text{Nd}$  ratios are estimated precise to  $\sim 2\%$  for kimberlite samples and better than  $0.5\%$   
278 for chloride-carbonates samples.

279

280

## 281 **4.3 Stable isotopes**

282

### 283 *Sulfur isotope analyses by chemical extraction and gas source mass spectrometry*

284 Sulfides and sulfates were extracted by wet chemistry using the sequential extraction  
285 procedure described in Kitayama et al. (2017). This sequential method (i.e. S extraction from  
286 sulfides using HCl and a chromium reducing solution, followed by S extraction from sulfate  
287 using a strongly reducing hydriodic hypophosphorous acid, in the same digestion flask)  
288 enables us to extract sulfides and sulfates from the same powder aliquot, thus also giving a  
289 measurement of their respective proportions. S isotope ratio measurements were carried out at  
290 the IPGP (Institut de Physique du Globe Paris) using a fluorination line to convert the  
291 extracted Ag<sub>2</sub>S to SF<sub>6</sub> gas. After separation and purification, the SF<sub>6</sub> gas was analyzed using a  
292 dual inlet ThermoFinnigan MAT 253 isotope ratio mass spectrometer (Thomassot et al.,  
293 2015). Sulfur isotope measurements are reported in the  $\delta$  notation with respect to V-CDT  
294 (Vienna-Canon Diablo Troilite) defined as:

$$295 \quad \delta^{34}\text{S} \text{ (in } \text{‰ V-CDT}) = 1000 * [({}^{34}\text{S}/{}^{32}\text{S})_{\text{sample}} / ({}^{34}\text{S}/{}^{32}\text{S})_{\text{V-CDT}} - 1]$$

296 The standard deviation of the  $\delta^{34}\text{S}$  values was calculated as the quadratic sum of the internal  
297 and external errors. The internal standard deviation calculated for each sample ( $2\sigma_{\text{int}}$ ) is  
298 0.05‰ for  $\delta^{34}\text{S}$ . During our sessions, the standard IAEA-S3 was measured 12 times, giving an  
299 external error ( $2\sigma_{\text{ext}}$ ) of 0.38‰ for  $\delta^{34}\text{S}$ .

300

301

## 302 **5. Results**

303

### 304 **5.1. Major and trace element compositions**

305

306 Major element compositions are reported in Table 2 and presented in Figure 3. Three salty  
307 kimberlite samples have on average, 30 wt.% MgO, 8.5 wt.% CO<sub>2</sub>, 26 wt.% SiO<sub>2</sub>, 8 wt.%  
308 FeO<sub>total</sub> and their major element compositions are consistent with a mixture between olivine,  
309 alkali-carbonates and chlorides. One sample (UV12-119; Table 2) deviates from the general  
310 trend, indicating a possible contribution from phlogopite (Fig. 3-a, -b). Chloride-carbonate  
311 nodules have from 17 to 19 wt.% CO<sub>2</sub>, 10 to 14 wt.% CaO, 18 to 23 wt.% Na, 9 to 11 wt.%  
312 K, 1 to 5 wt.% S and 17 to 31 wt.% Cl. Such major element compositions reflect the presence  
313 of alkali-carbonates (e.g., shortite and/or nyerereite), chlorides (mainly halite) and alkali-

314 sulfates (e.g., aphtitalite; Fig. 3). Compared to chloride-carbonate nodules, chlorides from  
315 hydrothermal veins and brine deposits have higher Na (from 36.3 to 39.4 wt.%) and lower K  
316 (<0.3 wt.%) contents (Table 2, Fig. 3). In contrast, the host sediment differs from the nodules  
317 in being poor in alkalis (K + Na < 0.1 wt.%) and Cl (~ 0.35 wt. %) despite S and Ca contents  
318 similar to those of chloride-carbonate nodules.

319 Salty kimberlites from Udachnaya are enriched in alkalis, chlorine and sulfur  
320 compared to non-salty kimberlites and other Siberian kimberlites (Figs. 3-d, -e and -f), and  
321 thus record a larger contribution from alkali-carbonates and chlorides. Rb contents of  
322 chloride-carbonate nodules are poorly correlated with Ca (Fig. 4-a) and CO<sub>2</sub> (Fig. 4-d),  
323 indicating that carbonates are not the only phases containing Rb. Rb contents of nodules are  
324 also inversely correlated with both Na (Fig. 4-b) and Cl (Fig. 4-e) while halite is generally  
325 Rb-poor (e.g., Schock and Puchelt, 1971). The only positive correlations of Rb contents are  
326 with K (Fig. 4-c) and S (Fig. 4-f), suggesting that Rb is associated to chloride (sylvite),  
327 carbonate ((shortite or/and nyerereite) and sulfate (aphtitalite) phases. In salty kimberlites,  
328 chloride carbonate nodules and chloride nodules, Sr is positively correlated with CO<sub>2</sub> (Fig. 4-  
329 g) and Ca, with a trend towards alkali-carbonate compositions (Kamenetsky et al., 2007),  
330 therefore Sr is largely held within carbonate minerals. Moreover, chloride-carbonate nodules  
331 show a trend of decreasing Sr with increasing Cl (Fig. 4-h) and Na + K contents (Fig. 4-i)  
332 indicating that Sr is not held within chloride or alkali-sulfate (aphtitalite).

333 Trace element compositions are presented in Table 3 and Figure 5. Kimberlites tend to  
334 be enriched in the more incompatible trace elements compared to primitive mantle and thus  
335 display steep trace element patterns, except for depletions in Cs, Rb, U, Pb and Ti (Fig. 5-a).  
336 In contrast, chloride-carbonate nodules are depleted in most trace elements compared to  
337 kimberlites but display marked enrichments in Rb, Pb and Sr, up to concentrations higher than  
338 those of the kimberlites (Fig. 5-b). Brine salts and hydrothermal salt veins barely contain any  
339 trace element (< detection limit or ≤ 1ppm) except for Ba, Cr, Pb, Rb, Sr and V (Table 3) and  
340 they are enriched in Rb, Pb and Sr (Fig. 5-c). The trace element pattern of the host Chukuck  
341 sediment differs from those of other samples in that its base is not subparallel to the  
342 kimberlite pattern and shows enrichments in Ba, U, Pb, extremely high Sr contents and a  
343 depletion in Rb (Fig. 5-d).

344

## 345 **5.2 Radiogenic isotopes (Rb-Sr, Sm-Nd)**

346

### 347 **5.2.1. Rb-Sr isotopes**

348

349 Results of Rb-Sr isotopes are reported in Table 4. Chloride-carbonate nodules have whole-  
350 rock  $^{87}\text{Sr}/^{86}\text{Sr}$  ratios of 0.707. Salty kimberlite samples have whole-rock  $^{87}\text{Rb}/^{86}\text{Sr}$  ratios  
351 ranging from 0.10 to 0.49 and  $^{87}\text{Sr}/^{86}\text{Sr}$  ratios ranging from 0.70435 to 0.70739.

352 In order to account for the difference in the Rb/Sr ratios, we have calculated the  
353  $^{87}\text{Sr}/^{86}\text{Sr}$  ratio at the time of kimberlite eruption ( $^{87}\text{Sr}/^{86}\text{Sr}_{365\text{Ma}}$ ). The mean  $^{87}\text{Sr}/^{86}\text{Sr}_{365\text{Ma}}$  of  
354 chloride-carbonate nodules is  $0.7055 \pm 0.0004$  ( $2\sigma$ ,  $n=2$ ), similar to the  $^{87}\text{Sr}/^{86}\text{Sr}_{365\text{Ma}}$  of the  
355 kimberlite (0.7038 to 0.7050;  $n=4$ ; Fig. 6-a). In comparison, the brine has an  $^{87}\text{Sr}/^{86}\text{Sr}_{365\text{Ma}}$  of  
356 0.7088. For the host sediment, we could not dissolve the silicate residue entirely so we could  
357 not obtain a whole-rock analysis. The acetic acid leachate of the host sediment, which  
358 represent  $\sim 71\%$  of the whole rock, has an  $^{87}\text{Sr}/^{86}\text{Sr}_{365\text{Ma}}$  of 0.7088, identical to the brine  
359 sample.

360 For spiked whole-rock samples of salty kimberlites, the use of Sr-spec resin for  
361 column separation failed to separate Rb and Sr effectively enough and thus, no Rb  
362 concentrations could be determined by isotopic dilution. Concentrations measured by isotopic  
363 dilution are usually within uncertainty of those measured on a different aliquot by ICP-MS at  
364 the SARM laboratory (Fig. 7). Only for whole-rock chloride-carbonate nodules, Rb  
365 concentrations measured by isotopic dilution were 30-40% higher than those measured ICP-  
366 MS at the SARM laboratory (Fig. 7-a). The most likely explanation is that the chemical  
367 composition of the rock matrix (Rb-rich alkali-carbonate and chloride) is very different from  
368 that of standard material used at the SARM laboratories, making the calibration less accurate.  
369 Salty kimberlites are not as rich in alkali-carbonate and chloride as the nodules, thus, for  
370 whole-rock salty kimberlites, we assume that Rb concentrations measured at the SARM  
371 laboratory (Table 3) are within uncertainty of the Rb concentrations that would be measured  
372 by isotopic dilution and use these values in further calculations (Table 4).

373

### 374 ***5.2.2. Sm-Nd isotopes***

375

376 Results of Sm-Nd isotopes are reported in Table 5 for chloride-carbonate nodules ( $n=2$ ) and  
377 salty kimberlite samples ( $n=4$ ). Whole-rock concentrations in Sm and Nd measured by  
378 isotopic dilution are within uncertainty of the concentrations measured by ICP-MS at the  
379 SARM laboratory (Table 3; Fig. 7-c and -d). All epsilon Nd values are reported at the time of  
380 kimberlite eruption, 365Ma.

381 Chloride-carbonate nodules have marginally radiogenic Nd isotope values, with  
382 epsilon Nd values of  $2.0 \pm 4.7$  and  $5.2 \pm 2.9$  that overlap with those of the salty kimberlite  
383 (from  $3.1 \pm 0.2$  to  $4.6 \pm 0.2$ ). The acetic acid leachate of the host sediment is less radiogenic  
384 with an epsilon Nd value of  $-4.5 \pm 3.6$ .

385

### 386 **5.3 Sulfur abundances, speciation (sulfide, sulfate) and isotopes ( $\delta^{34}\text{S}$ )**

387

388 Results of sulfur contents, speciation (sulfide or sulfate) and isotopes ( $\delta^{34}\text{S}$  in ‰ vs V-CDT) are  
389 reported in Table 6. Chloride-carbonate nodules are the most sulfur-rich samples, with up to  
390 ~3.9 wt% S, whereas salty kimberlites samples contain up to 0.30 wt% S. The veined  
391 sediment also has very high sulfur content (1.7 wt% S). In contrast, only ~31 ppm of S was  
392 extracted from the regional brine, which corresponds to 180 ppm if all the measured  
393 elemental concentrations are normalized to 100 atomic wt.% (see notes in Tables 2 and 3).  
394 Sulfur extractions were also applied to hydrothermal salt veins and salts precipitated from  
395 brines, but no sulfur could be extracted. Sulfur in the salt nodules is oxidized, with sulfate  
396 representing more than 99% of total sulfur while this proportion drops down to ~90% in the  
397 salty kimberlites. Isotopic compositions of sulfides are similarly depleted in  $^{34}\text{S}$  relative to V-  
398 CDT in chloride-carbonate nodules (with  $\delta^{34}\text{S}$  ranging from -2.7 to -1.2‰) and salty  
399 kimberlites (with  $\delta^{34}\text{S}$  ranging from -2.8 to -0.4‰; Fig. 8-a). Importantly, sulfates of chloride-  
400 carbonate nodules ( $\delta^{34}\text{S}$  ranging from 11.5 to 11.9‰) and salty kimberlites ( $\delta^{34}\text{S}$  ranging from  
401 11.2 to 11.9‰) have the same S isotopic compositions, significantly lower than those of the  
402 host sedimentary rock (Chukuck suite) and local brine samples (with both  $\delta^{34}\text{S}$  of 34‰; Fig.  
403 8).

## 404 6. Discussion

405

### 406 6.1. Why the Cambrian sedimentary cover is not the source of chloride-carbonate 407 nodules

408

409 Chloride-carbonate nodules are much more enriched in alkalis ( $\text{Na}+\text{K} > 20 \text{ wt.}\%$ , Fig. 3-d, -e  
410 and -f) and Cl (Fig. 3-e) compared to the wall-rock Chukuck sediment ( $0.10 \text{ wt.}\%$  Na+K and  
411  $0.35 \text{ wt.}\%$  Cl). They are also more enriched in S (1 to 5 wt.%) compared to the Chukuck  
412 sediment ( $1.7 \text{ wt.}\%$  S) or brine precipitates ( $\text{S} \leq 0.11 \text{ wt.}\%$ ; Fig. 3-d), thus Cambrian Chukuck  
413 suite sediments and brines cannot be their only sulfur source.

414 In terms of trace elements, hydrothermal veins and brine precipitates (Fig. 5-c) are  
415 depleted in all trace elements compared to chloride-carbonate nodules (Fig. 5-b) so they  
416 cannot represent a source of trace elements to the nodules. The Chukuck suite sediment is  
417 more enriched in trace elements than hydrothermal vein and brine precipitates, but its pattern  
418 is distinct from those of chloride-carbonate nodules in having flatter and more enriched heavy  
419 rare earth elements (HREE), a larger Sr enrichment, smaller Pb enrichment, U and Ba  
420 enrichments and the absence of Rb enrichment (Fig. 5-d).

421 From an isotopic point of view,  $^{87}\text{Sr}/^{86}\text{Sr}_{365\text{Ma}}$  of bulk chloride-carbonate nodules  
422 ( $0.7055 \pm 0.0004$ ;  $2\sigma$ ,  $n=2$ ; Table 4, Fig. 6-a) are significantly lower than the regional brine  
423 and country-rock sediment analysed in the present study ( $^{87}\text{Sr}/^{86}\text{Sr}_{365\text{Ma}} = 0.7088$ , Table 4, Fig.  
424 6-a) or reported in previous works (Zaitsev et al., 1985 in Kopylova et al., 2013). Just like Sr  
425 isotopes, sulfur signatures are significantly different in the country-rocks and in the chloride-  
426 carbonate nodules. Sulfates extracted from the nodules have  $\delta^{34}\text{S}$  from 11.5 to 11.9‰, within  
427 the compositional range of their host salty kimberlites ( $\delta^{34}\text{S}_{\text{sulfate}}$  from 9.2 to 12.0‰; Kitayama  
428 et al., 2017; Fig. 8-a). These sulfate compositions are lower than those of the Chukuck suite  
429 sediment (33.5‰), regional brine (33.7‰), hydrothermal sulfate minerals (15.6 to  
430 34.3‰; Kitayama et al., 2017), and much lower than any country-rock sediment of the  
431 Siberian platform ( $\geq 25\%$ ; Kitayama et al., 2017 and Vinogradov and Ilupin, 1972 in  
432 Kopylova et al., 2013; Fig. 8). Taken together, Sr and S isotopes indicate that chloride-  
433 carbonate nodules are neither xenoliths of Cambrian sediments nor precipitates from  
434 hydrothermal fluids.

435 To further test the possible contribution (even minimal) of Cambrian surficial material  
436 in the bulk composition of the nodules, one can use mixing calculations. In Fig. 8-b, mixing  
437 between the sulfate-rich wall-rock sediment of the Chukuck suite and the salty kimberlite

438 endmember would lead to a concave mixing trend (because  $[Sr]/[S]$  is 3 times higher in the  
439 kimberlite than in the sediment). However, in such a diagram as presented in Fig 8-b, salty  
440 kimberlite and chloride-carbonate samples display a horizontal trend of increasing  $^{87}Sr/^{86}Sr$   
441 ratios at a constant  $\delta^{34}S$ , unlike this mixing trend.

442 Similarly, we have considered a possible contribution from the local brine. Mixing  
443 calculations of kimberlite material with  $\leq 30\%$  of this brine produce a horizontal trend of  
444 increasing  $^{87}Sr/^{86}Sr$  ratios at a constant  $\delta^{34}S$ . If true, the nodule should have an intermediate  
445 composition lying between the brine and the kimberlite endmembers, in all compositional  
446 spaces. This is not consistent with the trend observed in  $\delta^{34}S$  vs  $1/[S]$  (Fig 8-c). In this  
447 graphical space, kimberlites are the samples with intermediate composition. Based on this  
448 observation, we can rule out a contribution from any known surficial reservoir in the genesis  
449 of chloride-carbonate nodules. Their sulfates represent the endmember compositions of  
450 kimberlitic sulfates observed in the salty kimberlites of the Udachnaya-East pipe.

451 These kimberlitic sulfates must come from a source that has yet to be identified, below  
452 the Cambrian sedimentary cover. In the absence of a known crustal component with such a  
453 signature, we further explore the interpretation that these characteristics are derived from the  
454 mantle source of kimberlites.

455

456

## 457 **6.2. A late-stage chloride-carbonate liquid, segregated from the evolving kimberlite**

458

459 One of the most remarkable features of kimberlites worldwide is their very similar trace  
460 element patterns (Khazan & Fialko, 2005, Giuliani et al., 2020). This similarity is interpreted  
461 to reflect that even kimberlites with highly variable major element compositions had a  
462 broadly similar parental melt before lithosphere assimilation. They would either derive from  
463 similar sources or have equilibrated with a common mantle component (Tappe et al., 2018;  
464 Giuliani et al., 2020). If the broad similarity between all kimberlites is accepted, the origin  
465 and the nature of their mantle source remain unclear. In particular, trace element patterns of  
466 kimberlites worldwide display some systematic depletions in K, Rb, Pb and Sr (Khazan &  
467 Fialko, 2005), which have yet to be fully discussed and explained.

468 Chloride-carbonate nodules from the Udachnaya-East kimberlite display extreme  
469 enrichments in Rb, Pb and Sr, while the distribution of other trace elements is subparallel to  
470 that in salty kimberlites, with the same base-line trend of trace element enrichments albeit at  
471  $\sim 2$  orders of magnitude lower in abundances compared to kimberlite samples (Fig. 5-b). Only

472 carefully chosen portions from the core parts of the nodules were analyzed, in order to  
473 minimize the effect of a possible contamination by the host kimberlite. Chloride-carbonate  
474 nodules are extremely enriched in K, Rb, Pb and Sr. In fact, they appear as the perfect  
475 counterparts of their host kimberlite, which are depleted in K, Rb, Pb and Sr. This suggests  
476 that the chloride-carbonate nodules may be linked to their host kimberlite by a process that  
477 led to the selective fractionation of these specific elements. To explain the subparallel base-  
478 line, as well as the marked enrichments in Rb, Pb and Sr in the chloride-carbonate nodules  
479 (Fig. 5-b), we propose that they were formed by the segregation of a chloride-carbonate  
480 liquid. The nodules are essentially composed of chloride and carbonates, and they are much  
481 more enriched in alkalis (Na + K), Cl and S compared to salty kimberlites (Fig. 3-d and -e).  
482 Rb is compatible in chloride, alkali-carbonate and perhaps also sulfur-bearing phases (Fig. 4-a  
483 to -f), whereas Sr is compatible in alkali-carbonate (Fig. 4-g, -h and -i) and Pb is a soluble and  
484 chalcophile element that also fits well into carbonates (as  $Pb^{2+}$ ). Therefore, the striking  
485 enrichments of the chloride-carbonate nodules in Rb, Sr and Pb above the contents observed  
486 in kimberlites (Fig. 5-b) as well as the slight depletions of the same elements in kimberlites  
487 (Fig. 5-a) are consistent with the chloride-carbonate nodules being a late-stage liquid,  
488 segregated from the evolving kimberlite.

489 This scenario is in agreement with the major element composition of salty kimberlites  
490 all falling within the mixing range of olivine (mantle or early liquidus), phlogopite (liquidus  
491 or metasomatized mantle) and chloride-carbonates (Fig. 3). The peculiar texture of chlorides  
492 and carbonates, reminiscent of immiscibility between alkaline-carbonate and alkaline-  
493 chloride liquids observed  $\sim 600^\circ\text{C}$  in melt inclusions trapped in olivine from the same  
494 kimberlite (Kamenetsky et al., 2004, 2007), suggests that chloride-carbonate nodules are  
495 snapshots of a liquid that was quenched  $\sim 600^\circ\text{C}$  at the closure of the kimberlite magma  
496 evolution. The convex pattern shaped by the relative abundances of light REE (from La to  
497 Sm) in Figure 9 as well as the smooth rise with increasing atomic number towards heavy REE  
498 is best explained by the crystallization of a phase enriched in light REE, such as apatite or  
499 perovskite, before the chloride-carbonate liquid exsolved. This is also consistent with a very  
500 late-stage segregation of the chloride-carbonate liquid from the kimberlite itself.

501 We propose that the trace-element patterns of kimberlites worldwide (Giuliani et al.,  
502 2020 and references therein) may also reflect the segregation a late-stage chloride-carbonate  
503 liquid. This hypothesis, however, is challenged by the apparent lack of "salty nodules" in most  
504 kimberlite-hosted deposits where major diamond mining operations retrieve very fresh and  
505 unaltered rocks (e.g., Siberia, Slave, Superior, Kaapvaal, Tanzania, Congo). Weathering and

506 dissolution of the nodules may explain that chloride-carbonate materials are missing in other  
507 localities. We did observe that alkali-carbonates and chlorides are extremely soluble and  
508 sensitive to changes in air moisture, even in the controlled environment of the laboratory.  
509 Nonetheless, some few kimberlite localities do have a coexisting discrete carbonate phase that  
510 can be interpreted as a product of kimberlite-carbonatite immiscibility at depth, or even as the  
511 coexistence of such distinctive components as primary liquids (Tappe et al., 2017; Howarth et  
512 al., 2019; Tappe et al., 2020a). These examples partially support our preferred model. If true  
513 this would imply a wider occurrence of chlorides and alkali-carbonates in kimberlites than  
514 previously thought.

515 At the time of kimberlite emplacement, chloride-carbonate nodules have epsilon Nd  
516 that overlap with those of their host salty kimberlites (Table 4, Fig. 6-b), kimberlitic  
517 perovskite from the same pipe/field (Kamenetsky et al., 2009; Sun et al., 2014) and more  
518 generally with other Siberian kimberlites (Carlson et al., 2006; Sun et al., 2014; Agashev et  
519 al., 2018) and Group I kimberlites from Southern Africa (Nowell et al., 2004; Smith, 1983;  
520 Tappe et al., 2020b; Fig. 6-b). Unlike Nd, it is generally accepted that Sr isotopes of  
521 kimberlites are easily overprinted during magma cooling in the presence of fluids and  
522 volatiles. This is best illustrated when comparing groundmass perovskite (with less radiogenic  
523  $^{87}\text{Sr}/^{86}\text{Sr}$ , Fig. 6-a) to their host kimberlite (whose  $^{87}\text{Sr}/^{86}\text{Sr}$  ratios extend to more radiogenic  
524 values at more or less unchanged epsilon Nd values, Fig. 6-b). A similar trend is observed in  
525 kimberlites from Western Greenland kimberlites (Fig. 4 in Tappe et al., 2012). It is worth  
526 noticing that the Sr isotope range in salty kimberlites is bracketed on one side by the  
527 perovskite composition (Kamenetsky et al., 2009), and on the other side by the chloride-  
528 carbonate nodule composition (Fig 6). We thus suggest that chloride-carbonate nodules  
529 represent the endmember fluid composition that stretches the range of Sr isotopic  
530 compositions in kimberlites to more radiogenic values. The aim of the following section is to  
531 explore the possible source(s) for the radiogenic isotope composition of these chloride-  
532 carbonate nodules.

533

534

### 535 **6.3. A high Rb/Sr component in the mantle sampled by kimberlites**

536

537 Pearson et al. (1995) have shown that peridotite xenoliths of the lithospheric mantle below the  
538 Udachnaya-East kimberlite pipe have heterogeneous radiogenic isotope composition (e.g.,  
539 epsilon Nd from -39.2 to + 8.2, Fig. 6-b). It seems unlikely then, that assimilation of dry

540 lithospheric material had a dominant impact in the clustered compositions found in salty  
541 kimberlites and associated nodules. Similarly, the continental crust of the Northeastern  
542 Siberian craton (Fig. 6-b; epsilon Nd =  $-22 \pm 4$  and  $^{87}\text{Sr}/^{86}\text{Sr} = 0.7126 \pm 0.0045$ , both  
543 recalculated at 365Ma; Rosen et al., 2006) is very distinct from the signatures observed in our  
544 samples and is thus not a likely source for the chloride-carbonate nodules. Instead, epsilon Nd  
545 of kimberlites and chloride-carbonate nodules (from +2 to +5.2) as well as their  $^{87}\text{Sr}/^{86}\text{Sr}$   
546 ratios (from 0.7038 to 0.7056), are both consistent with a moderately depleted mantle. These  
547 signatures may reflect a source in the ambient convecting upper mantle from which minor  
548 recycled components would be oversampled during low-degree partial melting. Although we  
549 cannot precisely define the specific type of sediments involved, they must have high Rb/Sr  
550 ratios in order to yield radiogenic Sr compositions over time. Such geochemical flavor with  
551 radiogenic Sr composition is comparable to what is found in some modern ocean island  
552 basalts (OIB) classified as enriched mantle 2 (EM2, e.g., Samoa, Hofmann, 2003; Fig. 6-b).  
553 The high  $^{87}\text{Sr}/^{86}\text{Sr}$  ratios of EM2 basalts has been interpreted by some authors as the recycling  
554 of terrigenous sediments (high Rb/Sr, Chauvel et al., 1992; Hofmann, 2003 and references  
555 therein), whereas the recycling of pelagic/carbonate-rich sediments (low Rb/Sr ratios) would  
556 lead over time to less radiogenic Sr-compositions such as observed in EM1-type basalts (Fig.  
557 6-b). The recycling of salts with very high Rb/Sr ratio, could also well explain the radiogenic  
558 Sr composition of salty kimberlites and chloride-carbonate nodules.

559 If not from the asthenosphere, the enrichment seen in kimberlites could have been  
560 acquired from alkalies, chlorine and sulfur-rich fluids that were percolating within the  
561 lithospheric mantle before being assimilated by the parental magma of the kimberlite (Francis  
562 and Patterson, 2009; Tappe et al., 2011; Guiliani et al., 2020). Metasomatism of the base of  
563 the lithospheric mantle, which would then initiate kimberlite magmatism, could have been  
564 fueled by the many subduction zones surrounding the Siberian continent in Neoproterozoic-  
565 Cambrian times, enriching the lithospheric mantle in volatile elements such as H<sub>2</sub>O and CO<sub>2</sub>  
566 (Kolesnichenko et al., 2017). This alternative hypothesis is supported by the presence of  
567 secondary melt inclusions in olivine from sheared peridotites at Udachnaya that equilibrated  
568 from 230 to 180 km depth (Golovin et al., 2018, 2020). These inclusions have trace element  
569 patterns with marked enrichments in Cs, Rb, Pb and Sr (Golovin et al., 2018) much like the  
570 chloride-carbonate nodules (Fig. 5-b).

571 Both scenarios (involving either an asthenospheric or lithospheric source of chlorides  
572 in kimberlite) are strongly supported by positive  $\delta^{37}\text{Cl}$  signatures recently reported in West  
573 Greenland kimberlite samples (Hoare et al., 2021) and by large quantities of halogens found

574 in the lithospheric mantle beneath the Udachnaya-East kimberlite (Broadley et al., 2018).  
575 These evidences support our hypothesis for the presence of a salt-rich component in the  
576 mantle sampled by kimberlites.

577

578

#### 579 **6.4. A mantle domain in which sulfates are dominant**

580

581 Sulfides of chloride-carbonate nodules (with  $\delta^{34}\text{S}$  ranging from -2.7 to -1.2‰) and salty  
582 kimberlites (with  $\delta^{34}\text{S}$  ranging from -2.8 to -0.4‰) have S-isotopic compositions consistent  
583 with mantle sulfides (MORB compositions of  $\sim -1\%$ , Labidi et al., 2013 and  $0 \pm 1.65\%$  for  
584 peridotitic sulfides from Udachnaya-East, Rudnick et al., 1993; Fig. 8-a). Similarly, sulfates  
585 of these nodules ( $\delta^{34}\text{S}$  ranging from 11.5 to 11.9‰) have the same S-isotopic compositions as  
586 sulfates from the salty kimberlite ( $\delta^{34}\text{S}$  ranging from 11.2 to 11.9‰), within the range of  
587 kimberlitic sulfates proposed by Kitayama et al., 2017; Fig. 8-a). These sulfate isotopic  
588 compositions correspond to the composition of sulfate in isotopic equilibrium with sulfide  
589 ( $\delta^{34}\text{S}$  of -1‰) at a temperature between 460°C and 570°C (Ohmoto and Rye, 1979; Miyoshi  
590 et al., 1984). Just like major, trace elements and radiogenic isotopes, S isotope systematics  
591 indicate that the chloride-carbonate nodules and salty kimberlites share a common mantle  
592 source, which retains mantle signatures instead of a signature contaminated by the Cambrian  
593 sedimentary cover.

594 The dominance of sulfate over sulfide in these nodules, as well as their S-isotopic  
595 composition provide some insights into the S-isotope composition of the mantle. Globally in  
596 the mantle, the isotope budget for reduced sulfur is not balanced: sulfides in mantle xenoliths,  
597 mid-ocean ridge basalts (Labidi et al., 2013, 2014) and in ocean island basalts (HIMU, Cabral  
598 et al., 2013; EM1, Delavault et al., 2016) all have  $\delta^{34}\text{S} < 0\%$ , when we expect balance to be  
599 achieved around the chondritic value of 0‰ (Canon Diablo Troilite). To explain this  
600 imbalance, it has been proposed that the depleted mantle itself has strictly negative  $\delta^{34}\text{S}$  ( $\sim -$   
601 1‰, Labidi et al., 2013, 2014). According to Labidi et al. (2013), this would result from  
602 isotopic fractionation during core-mantle segregation:  $^{34}\text{S}$  would have been preferentially  
603 dissolved in the core, leaving behind an excess of  $^{32}\text{S}$  in the mantle. Alternatively, sulfates  
604 with  $\delta^{34}\text{S} > 0\%$  stored in the mantle source of kimberlites could represent the missing  $^{34}\text{S}$   
605 reservoir needed to achieve mass balance at the planetary scale. Labidi et al. (2015) have  
606 suggested that oxidized sulfur in EM2-type lavas (from the ocean island of Samoa) could be  
607 the product of the interaction between magmatic water and reduced sulfur from the magma,

608 following the reaction:  $S^{2+} + 4H_2O = SO_4^{2-} + 4H_2$ . Although it is beyond the scope of this  
609 study, a similar reaction happening in the sulfur pool of the Udachnaya-East kimberlite,  
610 where most reduced sulfur becomes oxidized in a reaction with water, could be used to  
611 explain both the isotopic compositions of sulfates and the absence of water in the sulfate-rich,  
612 salty kimberlites.

613

614

## 615 **7. Conclusions**

616

### 617 *Chloride-carbonate nodules derived from the kimberlitic mantle source.*

618 The combination of major, trace element, Rb-Sr, Sm-Nd and S-isotopes indicates that  
619 chloride-carbonate nodules are magmatic products derived from a moderately depleted mantle  
620 source. Our results exclude the possibility that these chloride-carbonate nodules are xenoliths  
621 from the Cambrian sedimentary cover or crystallized from Cambrian brines infiltrating the  
622 kimberlite. They support the hypothesis that alkali-carbonates and their associated chlorides  
623 and sulfates in salty kimberlites have a mantle origin (either lithospheric or asthenospheric),  
624 tied to the genesis of their host kimberlite. Radiogenic isotope compositions indicate that a  
625 recycled component with high Rb/Sr (such as salts or terrigenous sediments) may be present  
626 in the mantle sampled by the salty kimberlite of Udachnaya-East, and perhaps of some other  
627 kimberlites as well. Such a component is consistent with the abundance of sulfates in the salty  
628 kimberlite and associated chloride-carbonate nodules.

629

### 630 *Segregation and preservation of the last-stage chloride-carbonate liquid of kimberlite.*

631 The trace element signatures of chloride-carbonate nodules can be explained by a  
632 magmatic fractionation during the segregation of a late-stage chloride-carbonate liquid from  
633 the rest of the kimberlite. This late-stage carbonate-chloride liquid was then quenched,  
634 resulting in a texture of intertwined chlorides and carbonates. Although most kimberlites  
635 worldwide are free of such distinct chloride-carbonate nodules, we propose that their  
636 strikingly similar trace element patterns (Khazan & Fialko, 2005, Giuliani et al., 2020) – in  
637 particular, their depletions in K, Rb, Pb and Sr – reflect the ghost signatures of such nodules  
638 and attest for their past existence in kimberlites worldwide.

639

640

641

Furthermore, in kimberlites worldwide, Sr isotopes display a range that extends to  
radiogenic Sr compositions at nearly constant Nd isotope values. The origin of such a range is  
most often interpreted as the result of overprint during magma cooling in the presence of

642 fluids (Tappe et al, 2012). However, in the absence of any sample of these hypothetical fluids,  
643 this interpretation has remained highly speculative. Based on their Nd-Sr isotope composition,  
644 here we propose that chloride-carbonate nodules are actually snapshots of these fluids,  
645 recording a missing compositional endmember.

646

647 ***An alternative hypothesis for the global imbalance of mantle sulfur.***

648 A mantle domain in which sulfate are dominant could partly explain why mantle  
649 sulfides do not match the chondritic value. Sulfate compositions in the chloride-carbonate  
650 nodules point toward a S isotope composition enriched in  $^{34}\text{S}$  ( $\delta^{34}\text{S}$  of +11‰) that correspond  
651 to the composition of sulfates in isotopic equilibrium with mantle sulfides ( $\delta^{34}\text{S}$  of -1‰) at the  
652 temperature at which nodules crystallized (~570°C). Such a  $^{34}\text{S}$ -enriched domain may explain  
653 the apparent imbalance observed between the chondritic value ( $\delta^{34}\text{S}$  of 0‰) and the negative  
654 compositions of both MORBs ( $\delta^{34}\text{S}$  of -1‰, Labidi et al., 2013, 2014) and peridotites ( $\delta^{34}\text{S}$  of  
655 -1‰, e.g., Rudnick et al., 1993).

656

657

658 **Acknowledgements**

659 The authors would like to thank Sebastian Tappe and two anonymous reviewers for their time  
660 and the quality of their critical comments that helped us improving the initial version of our  
661 manuscript, as well as Jeffrey G. Catalano and Rajdeep Dasgupta for the editorial handling.  
662 We are grateful to Catherine Zimmerman, Aimeryc Schumacher, Laurie Reisberg, Christiane  
663 Parmentier and Damien Cividini for their help in the clean lab and radiogenic isotope analyses  
664 at CRPG. Equally, we would like to thank Pierre Cartigny for granting us full access to the  
665 fluorination line and gas source mass-spectrometer for S-isotope measurements at IPGP while  
666 the CRPG fluorination line was not installed "yet". This work benefitted from the financial  
667 support of Agence Nationale de la Recherche to ET (ANR Dear-Sir; ANR-15-CE31-0005).  
668 Fieldwork at the Udachnaya mine, carried out by AVG and AVK, was supported by the  
669 Russian Federation state assignment of IGM SB RAS. This is contribution 2800 from CRPG.

670

671

672 **Research data:**

673 Research Data associated with this article can be accessed at:

674 <https://doi.org/10.24396/ORDAR-70>

675 Otelo research data repository (ORDaR) has been used for this contribution.

676

677

678 **References**

- 679 Abersteiner, A., Giuliani, A., Kamenetsky and V.S., Phillips, D. (2017). Petrographic and  
680 melt-inclusion constraints on the petrogenesis of a magmaclast from the Venetia  
681 kimberlite cluster, South Africa. *Chem. Geol.* **455**, 331-341.  
682 10.1016/j.chemgeo.2016.08.029
- 683 Abersteiner, A., Kamenetsky, V. S., Golovin, A. V., Kamenetsky, M., and Goemann, K.  
684 (2018). Was crustal contamination involved in the formation of the serpentine-free  
685 Udachnaya-East kimberlite? New insights into parental melts, liquidus assemblage and  
686 effects of alteration. *J. Petrol.* **59**(8), 1467-1492. 10.1093/petrology/egy068
- 687 Agashev, A. M., Nakai, S. I., Serov, I. V., Tolstov, A. V., Garanin, K. V., and Kovalchuk, O.  
688 E. (2018). Geochemistry and origin of the Mirny field kimberlites, Siberia. *Mineral.*  
689 *Petrol.* **112**(2), 597-608. 10.1007/s00710-018-0617-4
- 690 Alibert, C., Michard, A. and Albarède, F. (1983). The transition from alkali basalts to  
691 kimberlites: Isotope and trace element evidence from melilitites. *Contrib. to Mineral.*  
692 *Petrol.* **82**, 176–186. 10.1007/BF01166612.
- 693 Broadley, M. W., Barry, P. H., Ballentine, C. J., Taylor, L. A. and Burgess, R. (2018). End-  
694 Permian extinction amplified by plume-induced release of recycled lithospheric  
695 volatiles. *Nat. Geosci.* **11**(9), 682-687. 10.1038/s41561-018-0215-4
- 696 Brod, J. A., Junqueira-Brod, T. C., Gaspar, J. C., Petrinovic, I. A., de Castro Valente, S., and  
697 Corval, A. (2013). Decoupling of paired elements, crossover REE patterns, and  
698 mirrored spider diagrams: fingerprinting liquid immiscibility in the Tapira alkaline–  
699 carbonatite complex, SE Brazil. *J. South Am Earth Sci.* **41**, 41-56.  
700 10.1016/j.jsames.2012.04.013
- 701 Cabral, R.A., Jackson, M.G., Rose-Koga, E.F., Koga, K.T., Whitehouse, M.J., Antonelli,  
702 M.A., Farquhar, J., Day, J.M.D. and Hauri, E.H. (2013). Anomalous sulphur isotopes in  
703 plume lavas reveal deep mantle storage of Archaean crust. *Nature* **496**, 490–3.  
704 10.1038/nature12020
- 705 Carlson, R.W. and Czamanske, G., Fedorenko, V., Ilupin, I. (2006). A comparison of Siberian  
706 meimechites and kimberlites: Implications for the source of high-Mg alkalic magmas  
707 and flood basalts. *Geochem. Geophys. Geosyst.* **7**, 1–21. 10.1029/2006GC001342
- 708 Chauvel, C., Hofmann, A.W. and Vidal, P. (1992). HIMU-EM: The French Polynesian  
709 connection. *Earth Planet. Sci. Lett.* **110**, 99–119.
- 710 D'Eyramés, E., Thomassot, E., Kitayama, Y., Golovin, A., Korsakov, A. and Ionov, D.  
711 (2017). A mantle origin for sulfates in the unusual “salty” Udachnaya-East kimberlite  
712 from sulfur abundances, speciation and their relationship with groundmass carbonates.  
713 *Bulletin Société géologique de France*, **188**(1-2), 6. 10.1029/2005GC000919
- 714 Delavault, H., Chauvel, C., Thomassot, E., Devey, C. W. and Dazas, B. (2016). Sulfur and  
715 lead isotopic evidence of relic Archean sediments in the Pitcairn mantle plume. *Proc.*  
716 *Natl. Acad. Sci. U.S.A.* **113**(46), 12952-12956. 10.1073/pnas.1523805113
- 717 Fairchild, I. J., Borsato, A., Tooth, A. F., Frisia, S., Hawkesworth, C.J., Huang, Y. and Spiro,  
718 B. (2000). Controls on trace element (Sr–Mg) compositions of carbonate cave waters:

719 implications for speleothem climatic records. *Chem. Geol.* **166**(3-4), 255-269.  
720 10.1016/S0009-2541(99)00216-8

721 Francis, D. and Patterson, M. (2009). Kimberlites and aillikites as probes of the continental  
722 lithospheric mantle. *Lithos*, **109**(1-2), 72-80. 10.1016/j.lithos.2008.05.007

723 Giuliani, A., Soltys, A., Phillips, D., Kamenetsky, V. S., Maas, R., Goemann, K., Woodhead,  
724 J. D., Drysdale, R.N. and Grif, W. L. (2017). The final stages of kimberlite  
725 petrogenesis: Petrography, mineral chemistry, melt inclusions and Sr-C-O isotope  
726 geochemistry of the Bultfontein kimberlite (Kimberley, South Africa). *Chem. Geol.*  
727 **455**, 342–356. 10.1016/j.chemgeo.2016.10.011

728 Giuliani, A., Pearson, D. G., Soltys, A., Dalton, H., Phillips, D., Foley, S. F., Lim, E.,  
729 Goemann, K., Griffin, W. L. and Mitchell, R. H. (2020). Kimberlite genesis from a  
730 common carbonate-rich primary melt modified by lithospheric mantle assimilation. *Sci.*  
731 *Adv.* **6**(17), p.eaz0424. 10.1126/sciadv.aaz0424

732 Golovin, A. V., Sharygin, V. V. and Pokhilenko, N. P. (2007). Melt inclusions in olivine phe-  
733 nocrysts in unaltered kimberlites from the Udachnaya-East pipe, Yakutia: some aspects  
734 of kimberlite magma evolution during late crystallization stages. *Petrol.* **15**, 168–183.  
735 10.1134/S086959110702004X

736 Golovin, A. V., Sharygin, I. S., Kamenetsky, V. S., Korsakov, A. V. and Yaxley, G. M.  
737 (2018). Alkali-carbonate melts from the base of cratonic lithospheric mantle: Links to  
738 kimberlites. *Chem. Geol.* **483**, 261–274. 10.1016/j.chemgeo.2018.02.016

739 Golovin, A. V., Sharygin, I. S., Korsakov, A. V., Kamenetsky, V. S. and Abersteiner, A.  
740 (2020). Can primitive kimberlite melts be alkali-carbonate liquids: Composition of the  
741 melt snapshots preserved in deepest mantle xenoliths. *J. Raman Spectrosc.* **51**, 1849–  
742 1867. 10.1002/jrs.5701

743 Griffin, W. L. and O'Reilly, S. Y. (2007). Cratonic lithospheric mantle: is anything  
744 subducted? *Episodes*, **30**(1), 43-53.

745 Hoare, B. C., Tomlinson, E. L., Barnes, J. D., Tappe, S., Marks, M. A., Epp, T., Caulfield, J.,  
746 Riegler, T. (2021). Tracking halogen recycling and volatile loss in kimberlite  
747 magmatism from Greenland: Evidence from combined F-Cl-Br and  $\delta^{37}\text{Cl}$  systematics.  
748 *Lithos*, **384**, 105976. 10.1016/j.lithos.2021.105976

749 Hofmann, A. W. (2003). Sampling mantle heterogeneity through oceanic basalts: isotopes and  
750 trace elements. *Treatise on geochemistry*, **2**, 568.

751 Horwitz, E. P., Chiarizia R. and Dietz M. L. (1992). A novel strontium-selective extraction  
752 chromatographic resin. Solvent extraction and ion exchange, **10**(2), 313-336.  
753 10.1080/07366299208918107

754 Howarth, G. H., Moore, A. E., Harris, C., van der Meer, Q. H., & le Roux, P. (2019). Crustal  
755 versus mantle origin of carbonate xenoliths from Kimberley region kimberlites using  
756 CO-Sr-Nd-Pb isotopes and trace element abundances. *Geochimica et Cosmochimica*  
757 *Acta*, **266**, 258-273. doi.org/10.1016/j.gca.2019.03.026

758 Izraeli, E. S., Harris, J. W. and Navon, O. (2001). Brine inclusions in diamonds: a new upper  
759 mantle fluid. *Earth Planet. Sci. Lett.* **187**, 323–332. 10.1016/S0012-821X(01)00291-6

760 Jacob, D. E. and Foley, S. F. (1999). Evidence for Archean ocean crust with low high field  
761 strength element signature from diamondiferous eclogite xenoliths. *Dev. Geotecton.* **24**,  
762 317–336. 10.1016/S0419-0254(99)80017-2

763 Kamenetsky, M. B., Sobolev, A. V., Kamenetsky, V. S., Maas, R., Danyushevsky, L. V.,  
764 Thomas, R., Pokhilenko, N. P. and Sobolev, N. V. (2004). Kimberlite melts rich in  
765 alkali chlorides and carbonates: A potent metasomatic agent in the mantle. *Geology* **32**,  
766 845–848. 10.1130/G20821.1

767 Kamenetsky, V. S., Kamenetsky, M. B., Sharygin, V. V. and Golovin, A. V. (2007).  
768 Carbonate-chloride enrichment in fresh kimberlites of the Udachnaya-East pipe,

769 Siberia: A clue to physical properties of kimberlite magmas? *Geophys. Res. Lett.* **34**(9),  
770 L09316. 10.1029/2007GL029389

771 Kamenetsky, V.S., Kamenetsky, M.B., Sharygin, V. V., Faure, K. and Golovin, A. V. (2007).  
772 Chloride and carbonate immiscible liquids at the closure of the kimberlite magma  
773 evolution (Udachnaya-East kimberlite, Siberia). *Chem. Geol.* **237**, 384–400.  
774 10.1016/j.chemgeo.2006.07.010

775 Kamenetsky, V. S., Kamenetsky, M. B., Sobolev, A. V., Golovin, A. V., Demouchy, S.,  
776 Faure, K., Sharygin, V. V. and Kuzmin, D.V. (2008). Olivine in the Udachnaya-East  
777 Kimberlite (Yakutia, Russia): Types, Compositions and Origins, *J. Petrol.* **49**(4), 823–  
778 839. 10.1093/petrology/egm033

779 Kamenetsky, V. S., Maas, R., Kamenetsky, M. B., Paton, C., Phillips, D., Golovin, A. V and  
780 Gornova, M. A. (2009). Chlorine from the mantle: Magmatic halides in the Udachnaya-  
781 East kimberlite, Siberia. *Earth Planet. Sci. Lett.* **285**, 96–104.  
782 10.1016/j.epsl.2009.06.001

783 Kamenetsky, V. S., Golovin, A. V., Maas, R., Giuliani, A., Kamenetsky, M.B. and Weiss, Y.,  
784 (2014). Towards a new model for kimberlite petrogenesis: Evidence from unaltered  
785 kimberlites and mantle minerals. *Earth-Sci. Rev.* **139**, 145–167.  
786 10.1016/j.earscirev.2014.09.004

787 Kamenetsky, V. S., Kamenetsky, M. B., Golovin, A. V., Sharygin, V. V. and Maas, R.  
788 (2012). Ultrafresh salty kimberlite of the Udachnaya-East pipe (Yakutia, Russia): A  
789 petrological oddity or fortuitous discovery? *Lithos* **152**, 173–186.  
790 10.1016/j.lithos.2012.04.032

791 Kavanagh, J. L. and Sparks, R. S. J. (2009). Temperature changes in ascending kimberlite  
792 magma. *Earth Planet. Sci. Lett.* **286**, 404–413. 10.1016/j.epsl.2009.07.011

793 Khazan, Y., & Fialko, Y. (2005). Why do kimberlites from different provinces have similar  
794 trace element patterns? *Geochemistry, Geophysics, Geosystems*, *6*(10).  
795 10.1029/2005GC000919

796 Kinny, P. D., Griffin, B. J., Heaman, L. M., Brakhfogel, F. F. and Spetsius, Z. V (1997).  
797 SHRIMP U-Pb ages of perovskite from Yakutian kimberlites. *Geol. Geofiz.* **38**, 91–99  
798 (in Russian).

799 Kitayama, Y., Thomassot, E., Galy, A., Golovin, A., Korsakov, A., Assayag, N., Bouden, N.  
800 and Ionov, D. (2017). Co-magmatic sulfides and sulfates in the Udachnaya-East pipe (   
801 Siberia ): A record of the redox state and isotopic composition of sulfur in kimberlites  
802 and their mantle sources. *Chem. Geol.* **455**, 315–330. 10.1016/j.chemgeo.2016.10.037

803 Kjarsgaard, B. A., Pearson, D. G., Tappe, S., Nowell, G. M., & Dowall, D. P. (2009).  
804 Geochemistry of hypabyssal kimberlites from Lac de Gras, Canada: comparisons to a  
805 global database and applications to the parent magma problem. *Lithos*, *112*, 236-248.  
806 10.1016/j.lithos.2009.06.001

807 Klein-BenDavid, O., Izraeli, E. S., Hauri, E. and Navon, O. (2007). Fluid inclusions in  
808 diamonds from the Diavik mine, Canada and the evolution of diamond-forming fluids.  
809 *Geochim. Cosmochim. Acta* **71**(3), 723-744. 10.1016/j.gca.2006.10.008

810 Kolesnichenko, M., Zedgenizov, D.A., Litasov, K., Safonova, I. and Ragozin, A. (2016).  
811 Heterogeneous distribution of water in the mantle beneath the central Siberian Craton:  
812 Implications from the Udachnaya Kimberlite Pipe. *Gondwana Research* **47**, 249-266.  
813 [10.1016/j.gr.2016.09.011](https://doi.org/10.1016/j.gr.2016.09.011)

814 Kopylova, M.G., Gaudet, M., Kostrovitsky, S.I., Polozov, A.G. and Yakovlev D.A. (2016).  
815 Origin of salts and alkali carbonates in the Udachnaya East kimberlite: Insights from  
816 petrography of kimberlite phases and their carbonate and evaporite xenoliths. *J.*  
817 *Volcanol. Geotherm. Res.* **327**, 116-134. 10.1016/j.jvolgeores.2016.07.003

- 818 Kopylova, M. G., Kostrovitsky, S. I. and Egorov, K. N. (2013). Salts in southern Yakutian  
819 kimberlites and the problem of primary alkali kimberlite melts. *Earth-Sci. Rev.* **119**, 1–  
820 16. 10.1016/j.earscirev.2013.01.007
- 821 Labidi, J., Cartigny, P. and Jackson, M.G. (2015). Multiple sulfur isotope composition of  
822 oxidized Samoan melts and the implications of a sulfur isotope “ mantle array ” in  
823 chemical geodynamics. *Earth Planet. Sci. Lett.* **417**, 28–39. 10.1016/j.epsl.2015.02.004
- 824 Labidi, J., Cartigny, P. and Moreira, M. (2013). Non-chondritic sulphur isotope composition  
825 of the terrestrial mantle. *Nature* **501**, 208–11. 10.1038/nature12490
- 826 Labidi, J., Cartigny, P., Hamelin, C., Moreira, M. and Dosso, L. (2014). Sulfur isotope budget  
827 (<sup>32</sup>S, <sup>33</sup>S, <sup>34</sup>S and <sup>36</sup>S) in Pacific-Antarctic ridge basalts: A record of mantle source  
828 heterogeneity and hydrothermal sulfide assimilation. *Geochim. Cosmochim. Acta* **133**,  
829 47–67. 10.1016/j.gca.2014.02.023
- 830 Logvinova, A.M., Wirth, R., Fedorova, E.N. and Sobolev, N. V. (2008). Nanometer-sized  
831 mineral and fluid inclusions in cloudy Siberian diamonds: new insights on diamond  
832 formation. *Eur. J. Mineral.* **20**, 317–331. 10.1127/0935-1221/2008/0020-1815
- 833 Maas, R., Kamenetsky, M.B., Sobolev, A. V., Kamenetsky, V.S. and Sobolev, N. V. (2005).  
834 Sr, Nd, and Pb isotope evidence for a mantle origin of alkali chlorides and carbonates in  
835 the Udachnaya kimberlite, Siberia. *Geology* **33**, 549–552. 10.1130/G21257.1
- 836 Martin, L. H., Schmidt, M. W., Mattsson, H. B. and Guenther, D. (2013). Element  
837 partitioning between immiscible carbonatite and silicate melts for dry and H<sub>2</sub>O-bearing  
838 systems at 1–3 GPa. *J. Petrol.* **54**(11), 2301–2338. 10.1093/petrology/egt048
- 839 Michard, A., Gurriet, P., Soudant, M. and Albarede, F. (1985). Nd isotopes in French  
840 Phanerozoic shales: external vs. internal aspects of crustal evolution. *Geochim.*  
841 *Cosmochim. Acta* **49**, 601–610. 10.1016/0016-7037(85)90051-1
- 842 Miyoshi, T., Sakai, H., Chiba, H. (1984). Experimental study of sulfur isotope fractionation  
843 factors between sulfate and sulfide in high temperature melts. *Geochem. J.* **18**, 75–84.
- 844 Nowell, G. M., Kempton, P. D., & Pearson, D. G. (1998, April). Hf-Nd isotope systematics of  
845 kimberlites: relevance to terrestrial Hf-Nd systematics. In *International Kimberlite*  
846 *Conference: Extended Abstracts* (Vol. 7, pp. 628-630).
- 847 Nowell, G. M., Pearson, D. G., Bell, D. R., Carlson, R. W., Smith, C. B., Kempton, P. D. and  
848 Noble, S. R. (2004). Hf Isotope Systematics of Kimberlites and their Megacrysts: New  
849 Constraints on their Source Regions. *J. Petrol.* **45**, 1583–1612.  
850 10.1093/petrology/egh024
- 851 Ohmoto, H., Rye, R.O. (1979). Isotopes of sulfur and carbon. In: Barnes, H.L. (Ed.),  
852 *Geochemistry of Hydrothermal Ore Deposits*, second ed. Wiley, New York, pp. 509–  
853 567.
- 854 Pearson, D. G., Snyder, G. A., Shirey, S. B., Taylor, L. A., Carlson, R. W. and Sobolev, N. V.  
855 (1995). Archaean Re–Os age for Siberian eclogites and constraints on Archaean  
856 tectonics. *Nature* **374**, 711–713. 10.1038/374711a0
- 857 Pearson, D. G., Shirey, S. B., Carlson, R. W., Boyd, F. R., Pokhilenko, N. P. and Shimizu, N.,  
858 (1995). Re–Os, Sm–Nd, and Rb–Sr isotope evidence for thick Archaean lithospheric  
859 mantle beneath the Siberian craton modified by multistage metasomatism. *Geochim.*  
860 *Cosmochim. Acta* **59**, 959–977. 10.1016/0016-7037(95)00014-3
- 861 Pin, C., Briot, D., Bassin, C. and Poitrasson, F. (1994). Concomitant separation of strontium  
862 and samarium-neodymium for isotopic analysis in silicate samples, based on specific  
863 extraction chromatography. *Anal. Chim. Acta* **298**, 209–217. 10.1016/0003-  
864 2670(94)00274-6
- 865 Pin, C., Francisco, J. and Zalduegui, S. (1997). Sequential separation of light rare-earth  
866 elements, thorium and uranium by miniaturized extraction chromatography: application

867 to isotopic analyses of silicate rocks. *Anal. Chim. Acta* **339**, 79–89. 10.1016/S0003-  
868 2670(96)00499-0

869 Pokrovsky, O. S., Golubev, S. V and Schott, J. (2005). Dissolution kinetics of calcite,  
870 dolomite and magnesite at 25°C and 0 to 50 atm pCO<sub>2</sub>. *Chem. Geol.* **217**, 239–255.  
871 10.1016/j.chemgeo.2004.12.012

872 Rudnick, R.L., Eldridge, C.S. and Bulanova, G.P. (1993). Diamond growth history from in  
873 situ measurement of Pb and S isotopic compositions of sulfide inclusions. *Geology* **21**,  
874 13–16.

875 Sharygin, I. S., Golovin, A. V and Pokhilenko, N. P. (2011). Djerfisherite in Kimberlites of  
876 the Kuoikskoe Field as an Indicator of Enrichment of Kimberlite Melts in Chlorine.  
877 *Dokl. Earth Sci.* **436**, 820–826. 10.1134/S1028334X11020255

878 Schock, H. H. and Puchelt, H. (1971). Rubidium and cesium distribution in salt minerals—I.  
879 Experimental investigations. *Geochim. Cosmochim. Acta*, **35**(3), 307-317.  
880 10.1016/0016-7037(71)90039-1

881 Smith, C. B. (1983). Pb, Sr and Nd isotopic evidence for sources of southern African  
882 Cretaceous kimberlites. *Nature* **304**, 51–54.

883 Sobolev, N. V, Logvinova, A.M. and Efimova, E.S. (2009). Syngenetic phlogopite inclusions  
884 in kimberlite-hosted diamonds: implications for role of volatiles in diamond formation.  
885 *Russ. Geol. Geophys.* **50**, 1234–1248. 10.1016/j.rgg.2009.11.021

886 Sun, J., Liu, C. Z., Tappe, S., Kostrovitsky, S. I., Wu, F. Y., Yakovlev, D., Yang, Y. H. &  
887 Yang, J. H. (2014). Repeated kimberlite magmatism beneath Yakutia and its  
888 relationship to Siberian flood volcanism: insights from in situ U–Pb and Sr–Nd  
889 perovskite isotope analysis. *Earth and Planetary Science Letters*, **404**, 283-295.

890 Tappe, S., Pearson, D. G., Nowell, G., Nielsen, T., Milstead, P., & Muehlenbachs, K. (2011).  
891 A fresh isotopic look at Greenland kimberlites: cratonic mantle lithosphere imprint on  
892 deep source signal. *Earth and Planetary Science Letters*, **305**(1-2), 235-248.  
893 10.1016/j.epsl.2011.03.005

894 Tappe, S., Steenfelt, A., & Nielsen, T. (2012). Asthenospheric source of Neoproterozoic and  
895 Mesozoic kimberlites from the North Atlantic craton, West Greenland: new high-  
896 precision U–Pb and Sr–Nd isotope data on perovskite. *Chemical Geology*, **320**, 113-  
897 127. 10.1016/j.chemgeo.2012.05.026

898 Tappe, S., Romer, R. L., Stracke, A., Steenfelt, A., Smart, K. A., Muehlenbachs, K., &  
899 Torsvik, T. H. (2017). Sources and mobility of carbonate melts beneath cratons, with  
900 implications for deep carbon cycling, metasomatism and rift initiation. *Earth and*  
901 *Planetary Science Letters*, **466**, 152-167. 10.1016/j.epsl.2017.03.011

902 Tappe, S., Smart, K., Torsvik, T., Massuyeau, M., & de Wit, M. (2018). Geodynamics of  
903 kimberlites on a cooling Earth: clues to plate tectonic evolution and deep volatile  
904 cycles. *Earth and Planetary Science Letters*, **484**, 1-14. 10.1016/j.epsl.2017.12.013

905 Tappe, S., Stracke, A., van Acken, D., Strauss, H., & Luguet, A. (2020a). Origins of  
906 kimberlites and carbonatites during continental collision—insights beyond decoupled  
907 Nd-Hf isotopes. *Earth-Science Reviews*, 103287. 10.1016/j.earscirev.2020.103287

908 Tappe, S., Budde, G., Stracke, A., Wilson, A., & Kleine, T. (2020b). The tungsten-182 record  
909 of kimberlites above the African superplume: Exploring links to the core-mantle  
910 boundary. *Earth and Planetary Science Letters*, **547**, 116473.  
911 10.1016/j.epsl.2020.116473

912 Thomassot, E., O’Neil, J., Francis, D., Cartigny, P. and Wing, B. A. (2015). Atmospheric  
913 record in the Hadean Eon from multiple sulfur isotope measurements in Nuvvuagittuq  
914 Greenstone Belt (Nunavik, Quebec). *Proc. Natl. Acad. Sci.* **112**(3), 707-712.  
915 10.1073/pnas.1419681112

- 916 Tomilenko, A. A., Dublyansky, Y. V., Kuzmin, D. V., & Sobolev, N. V. (2017a). Isotope  
917 compositions of C and O of magmatic calcites from the Udachnaya–East pipe  
918 kimberlite, Yakutia. *Doklady Earth Sci.* **475**, 828-831.
- 919 Tomilenko, A. A., Kuzmin, D. V., Bul'bak, T. A. and Sobolev, N. V. (2017b). Primary Melt  
920 and Fluid Inclusions in Regenerated Crystals and Phenocrysts of Olivine from  
921 Kimberlites of the Udachnaya-East Pipe, Yakutia: The Problem of the Kimberlite Melt.  
922 *Dokl. Earth Sci.* **475**, 949–952. 10.1134/S1028334X1708028
- 923 Weiss, Y., McNeill, J., Pearson, D.G., Nowell, G.M. and Ottley, C.J. (2015). Highly saline  
924 fluids from a subducting slab as the source for fluid-rich diamonds. *Nature* **524**, 339–  
925 342. 10.1038/nature14857
- 926 Workman, R.K., Hart, S.R., Jackson, M., Regelous, M., Farley, K.A., Blusztajn, J., Kurz, M.  
927 and Staudigel, H. (2004). Recycled metasomatized lithosphere as the origin of the  
928 Enriched Mantle II (EM2) end-member: Evidence from the Samoan Volcanic Chain.  
929 *Geochemistry, Geophysics, Geosystems*, 5(4). [10.1029/2003GC000623](https://doi.org/10.1029/2003GC000623)
- 930 Yang, Y., Galy, A., Fang, X., Yang, R., Zhang, W. and Zan, J. (2017). Eolian dust forcing of  
931 river chemistry on the northeastern Tibetan Plateau since 8 Ma. *Earth Planet. Sci. Lett.*  
932 **464**, 200–210. 10.1016/j.epsl.2017.02.009
- 933 Zedgenizov, D.A., Ragozin, A.L. and Shatsky, V.S. (2007). Chloride – carbonate fluid in  
934 diamonds from the eclogite xenolith. *Dokl. Earth Sci.* **415A**, 961–964.  
935 10.1134/S1028334X07060293
- 936 Zedgenizov, D. A., Ragozin, A. L., Shatsky, V. S. and Griffin, W. L. (2018). Diamond  
937 formation during metasomatism of mantle eclogite by chloride-carbonate melt. *Contrib.*  
938 *Mineral. Petrol* **173**(10), 84. 10.1007/s00410-018-1513-y
- 939 Zaitsev, A. I., Nikishov, K. N., Nenashev, N. I., & Kovalskiy, V. V. (1985). Evolution of Sr-  
940 isotope composition in kimberlite rocks of the Yakutian province. *Petrologic-  
941 geochemical characteristics of deep evolution of the matter of kimberlitic and basaltic  
942 magmatic systems. Yakutsk*, 13-37.

943 **Figure captions: (9 figures, provided as independent files)**

944

945 **Figure 1:** Map showing the distribution of kimberlite fields on the Siberian craton and the  
946 location of the Udachnaya-East kimberlite pipe relative to the extent of brine-bearing  
947 sediments and Cambrian saliferous sediments (modified after Sharygin et al., 2011).

948

949 **Figure 2:** Photographs of salt-bearing samples from the Udachnaya-East kimberlite pipe and  
950 area. Chloride-carbonate nodules and their host kimberlite, samples UV11-201 (a) and  
951 UV11-203 (b). Chloride-carbonate nodules show an intricate network of alternating chloride  
952 and carbonate sheets, interpreted as immiscibility textures formed during quenching. (c) Grey  
953 halite from a hydrothermal vein. (d) Hydrothermal vein with blue and clear halite showing  
954 smooth weathered surfaces, cutting through the kimberlite. (e) Country rock sediment of the  
955 Chukuck suite with a sulfate-rich vein, sample UV09-305. (f) Brine precipitates collected from  
956 520m depth in the open pit, where they have crystallized after the evaporation of brines,  
957 sample UV09-720 (pen for scale). (g) Brine collected at a depth of 750 m from a drill hole 1  
958 km south of Udachnaya (0.5 L bottle).

959

960 **Figure 3:** Major element compositions of samples from the Udachnaya-East kimberlite pipe  
961 and area, showing the contributions of silicate (e.g., olivine, phlogopite), carbonate (e.g.  
962 calcite, northupite, shortite, nyerereite), sulfate (e.g. aphtitalite) and chloride (e.g. halite,  
963 sylvite) compositions to the whole-rock compositions. (a, b, c) Olivine, phlogopite, chloride  
964 and carbonate (the mineral endmembers connected by grey lines) are the main constituents of  
965 kimberlites (red squares and white circles) from Udachnaya-East. (d, e, f) Aphtitalite, halite,  
966 and shortite (the alkali-minerals connected by grey lines) are the main constituents of  
967 chloride-carbonate nodules (purple diamonds with black rims). Other Siberian kimberlites  
968 are also shown for comparison (small grey circles).

969 *References:* [1] Kamenetsky et al., 2008; [2] Kamenetsky et al., 2009; [3] Kamenetsky et al.,  
970 2007; [4] This study, D'Eyrammes et al., 2017 and Kamenetsky et al., 2012; [5] Agashev et al.,  
971 2018.

972

973 **Figure 4:** Rb concentrations with respect to CaO (a), Na (b), K (c), CO<sub>2</sub> (d), Cl (e) and S (f)  
974 and Sr concentrations with respect to CO<sub>2</sub> (g), Cl (h) and Na + K (i) in mineral and whole  
975 rock compositions of samples from the Udachnaya-East kimberlite and area. The host

976 *sediment is outside the displayed range of Sr compositions. Other Siberian kimberlites are*  
977 *also shown for comparison.*

978 *References: [1] Kamenetsky et al., 2008; [2] Kamenetsky et al., 2007 – CO<sub>2</sub> contents were*  
979 *not included in the analyses of alkali-carbonate sheets so we estimated them assuming only*  
980 *CO<sub>2</sub> was missing from a total oxide wt.% of 100; [3] Kamenetsky et al., 2004; [4] This study,*  
981 *D'Eyrames et al., 2017 and Kamenetsky et al., 2012; [5] Agashev et al., 2018.*

982

983 **Figure 5:** *Trace element concentrations normalized to primitive mantle (McDonough and*  
984 *Sun, 1995), for salty kimberlites compared to kimberlites worldwide (a), chloride-carbonate*  
985 *nodules (b), hydrothermal salt veins and brine salts (c) and host sediment (d).*

986 *Reference: [1] Giuliani et al., 2020.*

987

988 **Figure 6:** *(a) <sup>87</sup>Sr/<sup>86</sup>Sr ratios calculated at 365 Ma chloride-carbonate nodules and salty*  
989 *kimberlites (both whole-rock compositions) from the Udachnaya-East pipe, compared to*  
990 *those of the Cambrian host sediment (acid leachate) and regional brine, as well as other*  
991 *ranges from the literature including Siberian sediments, Siberian kimberlites, kimberlitic*  
992 *perovskite and clinopyroxene from the Udachnaya-East pipe and the Daldyn kimberlite field,*  
993 *silicate residue of salty kimberlite from the Udachnaya-East pipe, peridotite xenoliths from*  
994 *the Udachnaya-East pipe, depleted mantle and enriched mantle. (b) Epsilon Nd vs <sup>87</sup>Sr/<sup>86</sup>Sr*  
995 *(at 365 Ma) of salty kimberlites (whole-rock and silicate residue) and chloride-carbonate*  
996 *nodules (whole-rock) of the Udachnaya-East pipe, as well as the Chukuck suite sediment of*  
997 *the Cambrian sedimentary cover (acetic acid leachate). Kimberlitic perovskite and*  
998 *clinopyroxene from the Udachnaya-East pipe and the Daldyn kimberlite field, peridotite*  
999 *xenoliths from Udachnaya-East, other Siberian kimberlites, Group I and Group II kimberlites*  
1000 *from Southern Africa are shown for comparison (the values displayed correspond to the*  
1001 *initial isotopic compositions, calculated at the time of each kimberlite eruption). Endmember*  
1002 *compositions of modern basalts (Hofmann, 2003), including the depleted MORB mantle*  
1003 *(DMM, epsilon Nd = +11 and <sup>87</sup>Sr/<sup>86</sup>Sr = 0.703 at 365 Ma) and enriched mantle (EM1,*  
1004 *epsilon Nd = -2 and <sup>87</sup>Sr/<sup>86</sup>Sr = 0.705 and EM2, epsilon Nd = +2 and <sup>87</sup>Sr/<sup>86</sup>Sr = 0.706, both*  
1005 *at 365 Ma), as well as the average continental crust from the Northeastern Siberian craton*  
1006 *(epsilon Nd = -22 ± 4 and <sup>87</sup>Sr/<sup>86</sup>Sr = 0.713 ± 0.005 at 365 Ma, outside the graphical range,*  
1007 *Rosen et al., 2006) are also shown for comparison.*

1008 *References: [1] Kostrovitsky et al., 1986 in Kopylova et al., 2013; [2] Nowell et al., 1998;*  
1009 *Agashev et al., 2018; Carlson et al., 2006; Sun et al., 2014; [3] Maas et al., 2005; [4]*

1010 Kamenetsky et al., 2009; Sun et al., 2014; [5] Pearson et al., 1995; [6] Zindler and Hart,  
1011 1986; Hofmann 2003; [7] Smith, 1983; Nowell et al., 2004; Tappe et al., 2020a; [8] Rosen et  
1012 al., 2006.

1013

1014 **Figure 7:** Rb (a), Sr (b), Sm (c) and Nd concentrations (d) of whole-rock samples measured  
1015 by acid digestion and isotopic dilution (ID) compared to the concentrations measured by  
1016 fusion and ICP-MS at the SARM laboratory. Concentrations obtained by the two methods are  
1017 within uncertainty, except for the Rb-contents of chloride-carbonate nodules due to their non-  
1018 conventional matrix compositions (Rb-rich alkali-carbonate).

1019

1020 **Figure 8:** Sulfur isotopic compositions ( $\delta^{34}\text{S}$ ) measured in sulfides and sulfates from salt-  
1021 bearing samples of the Udachnaya-East pipe: with respect to 1/[S] in wt.% (a) and with  
1022 respect to their  $^{87}\text{Sr}/^{86}\text{Sr}$  ratios at 365 Ma (b). Literature ranges for Siberian sediments (pale  
1023 yellow area), primitive mantle (black cross), MORB and peridotitic sulfides from the  
1024 Udachnaya-East pipe (green area) are shown for comparison. (a) Sulfides from chloride-  
1025 carbonate nodules (filled diamonds) and salty kimberlites (filled squares) are all within the  
1026 mantle range, whereas sulfates from chloride-carbonate nodules (open diamonds) and salty  
1027 kimberlites (open squares) define kimberlitic sulfate compositions. In plots of  $\delta^{34}\text{S}$  vs 1/[S],  
1028 binary mixing between two endmember compositions produces linear correlations between  
1029 them. Sulfates from chloride-carbonate nodules represent the endmember composition found  
1030 in salty kimberlites. They cannot be explained by mixing between other known sulfur sources.  
1031 (b) Sulfates dominate the sulfur budget of all samples, thus, only the sulfur isotopic  
1032 compositions of sulfates are represented. In plots of  $\delta^{34}\text{S}$  vs.  $^{87}\text{Sr}/^{86}\text{Sr}$  ratios, binary mixing  
1033 between two end-member compositions produces non-linear correlations between them. The  
1034 curvature of the mixing lines depends on the endmembers' relative S and Sr concentrations.

1035 References: [1] Kitayama et al., 2017; [2] Labidi et al., 2013, 2014; [3] Rudnick et al., 1993;  
1036 [4] McDonough and Sun, 1995; [5] Kostrovitsky et al., 1986 and Vinogradov and Ilupin,  
1037 1972 in Kopylova et al., 2013.

1038

1039 **Figure 9:** Rare Earth Element (REE) concentrations in the chloride-carbonate nodules  
1040 normalized to the average composition of salty kimberlites. The smooth rise in these ratios  
1041 with increasing atomic number of the REEs suggests either that chloride-carbonate nodules  
1042 equilibrated after the crystallization of a phase enriched in light REE (apatite being a good  
1043 candidate as we did observe it in kimberlite samples).

1044 **Table captions: (6 tables + 1 supplementary material, provided in an independent file)**

1045

1046 **Table 1:** Chloride fraction (in wt.%) estimated from major element compositions compared to  
1047 weighed proportions (in wt.%) of the water leachates, acid leachates and residual solids of the  
1048 leached samples.

1049

1050 **Table 2:** Major element compositions of salty kimberlites and chloride-carbonate nodules  
1051 from the Udachnaya-East pipe, as well as hydrothermal veins from the same pipe and salt-  
1052 bearing samples from the sedimentary cover.

1053

1054 **Table 3:** Trace element compositions of salty kimberlites and chloride-carbonate nodules  
1055 from the Udachnaya-East pipe, as well as hydrothermal veins from the same pipe and salt-  
1056 bearing samples from the sedimentary cover.

1057

1058 **Table 4:** Rb and Sr concentrations and isotopic compositions of nodules and samples from  
1059 the Udachnaya-East kimberlite pipe and area.

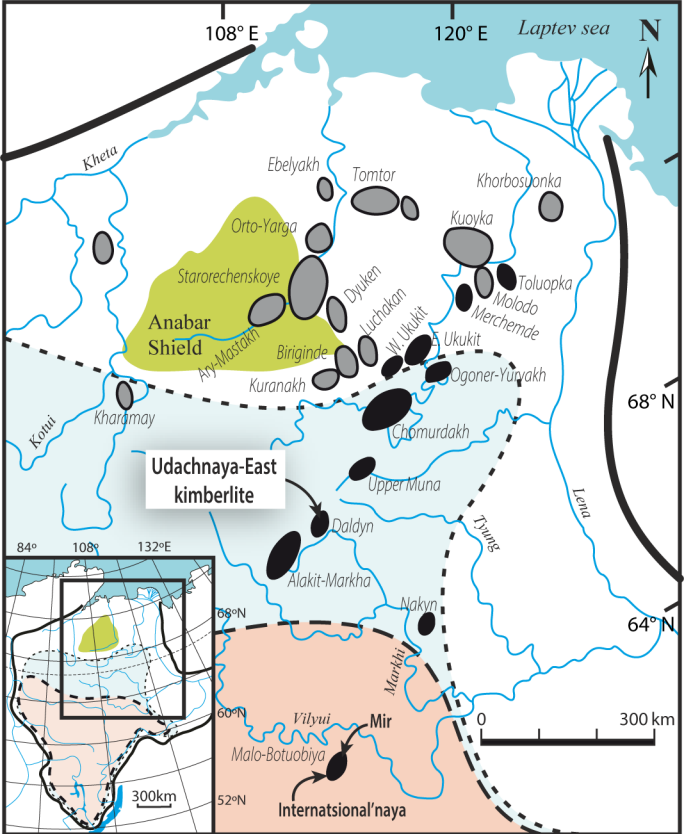
1060

1061 **Table 5:** Sm and Nd concentrations and isotopic compositions of nodules and samples from  
1062 the Udachnaya-East kimberlite pipe and area.

1063

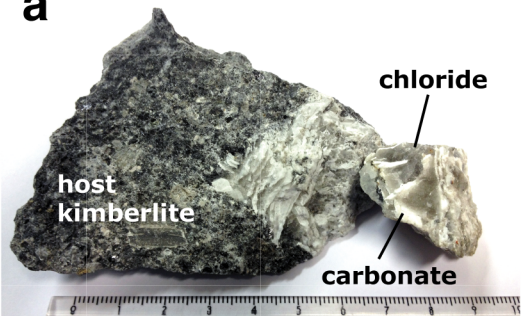
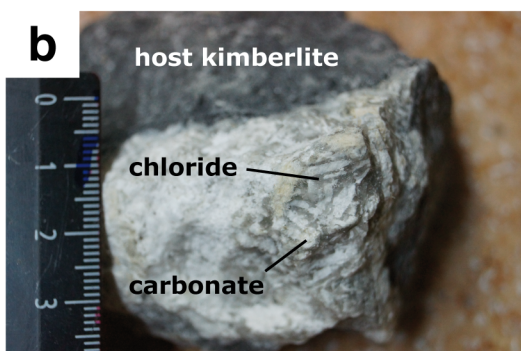
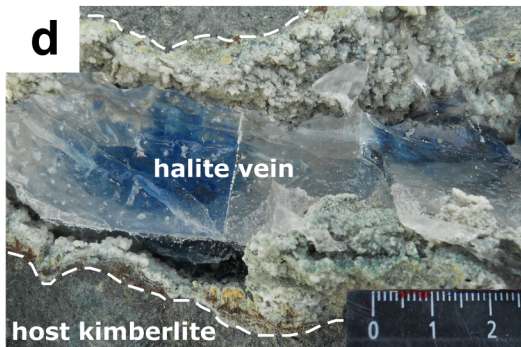
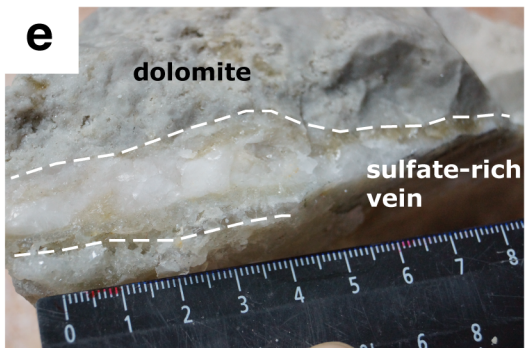
1064 **Table 6:** S concentrations and isotopic compositions (as sulfide and sulfate) of nodules and  
1065 other samples from the Udachnaya-East kimberlite and area.

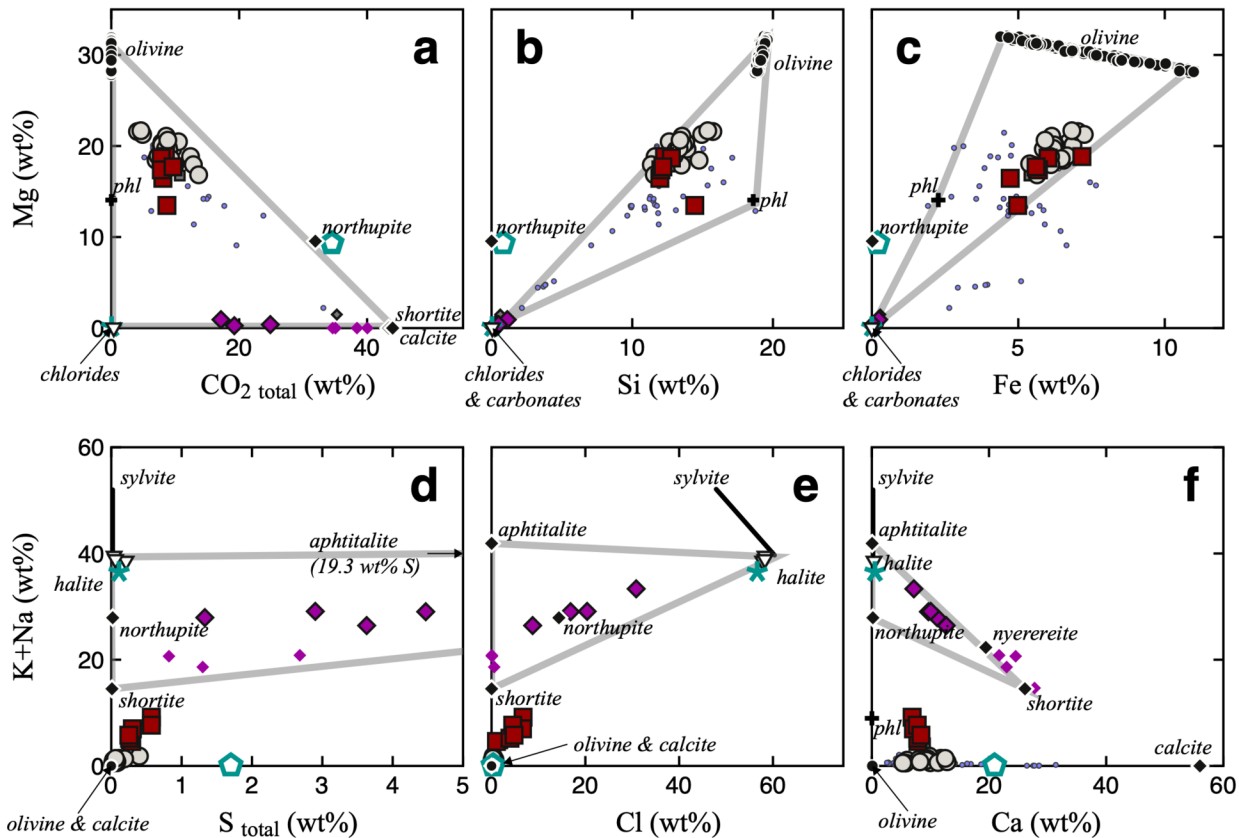
1066



-  Boundaries of the Siberian platform
-  Exposed basement of the Siberian craton
-  Cambrian saliferous sediments
-  Area of modern brines

- Kimberlite fields:**
-  Mesozoic (251 - 65.5 Ma)
  -  Paleozoic (542 - 251 Ma)

**a****b****c****d****e****f****g**

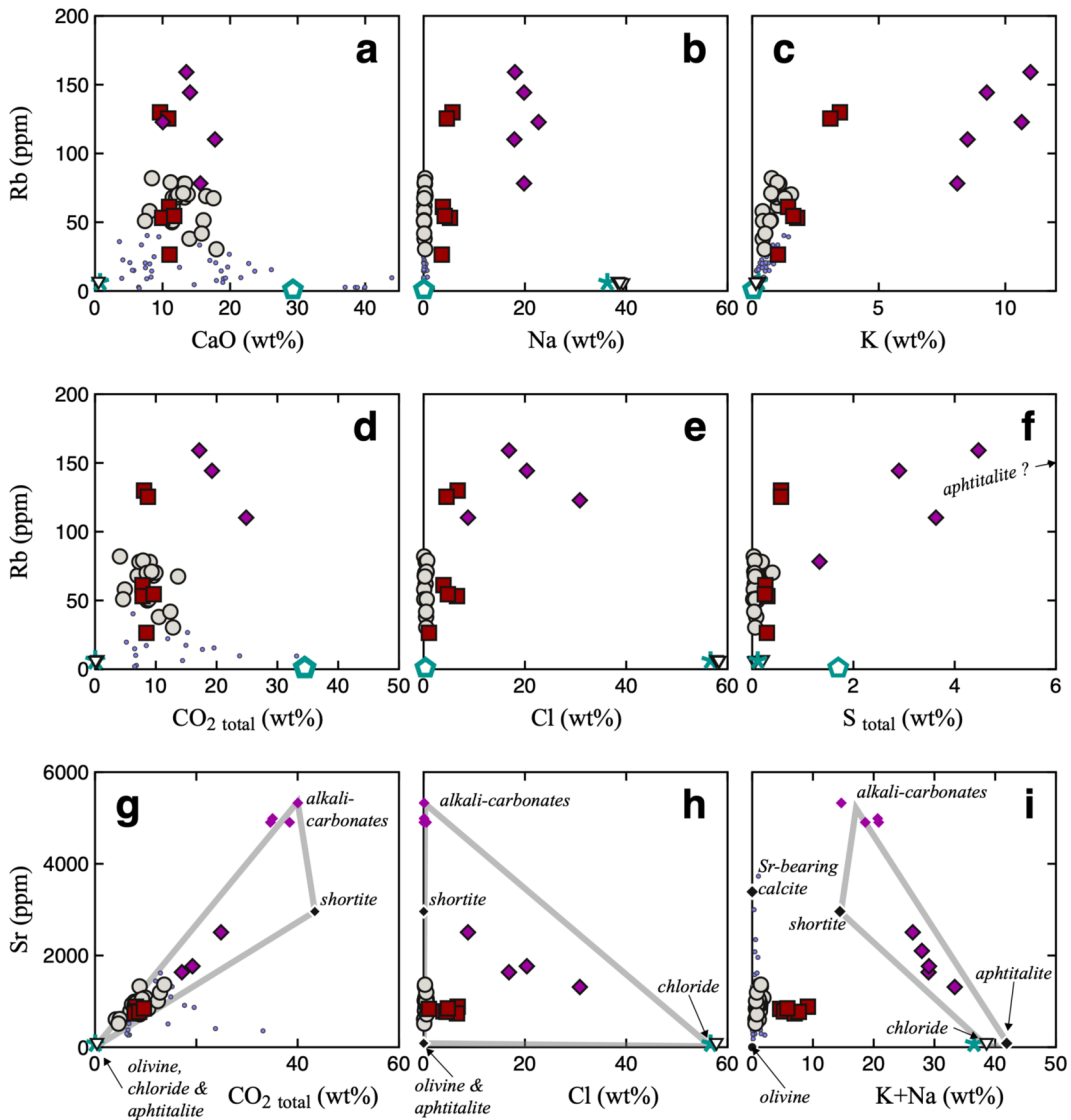


**Mineral compositions:**

- olivine <sup>[1]</sup>
- ◆ carbonate (calcite, shortite <sup>[3]</sup>, northupite <sup>[3]</sup>) and sulfate (aphtitalite <sup>[3]</sup>) compositions
- ◆ alkali-carbonate sheets <sup>[3]</sup>
- ◆ carbonates (calcite, shortite <sup>[3]</sup>, northupite <sup>[3]</sup>) and sulfate (aphtitalite <sup>[3]</sup>) compositions
- ◆ chloride (halite to sylvite)
- mixing

**Whole-rock compositions:**

- ◆ chloride-carbonate nodule
- salty kimberlite <sup>[4]</sup>
- non-salty kimberlite <sup>[4]</sup>
- siberian kimberlites <sup>[5]</sup>
- ▽ hydrothermal veins
- \* brine precipitates
- ◇ host sediment

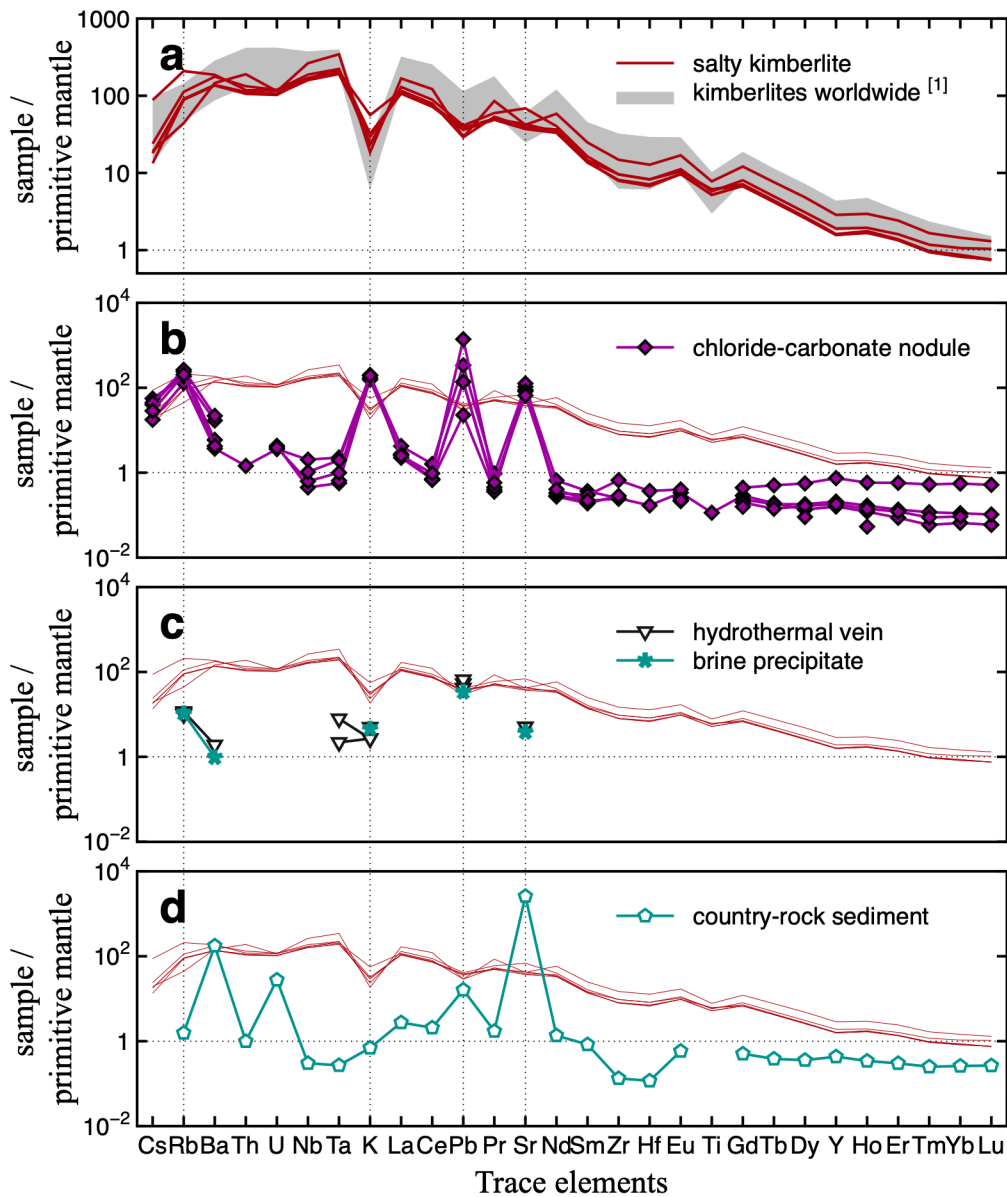


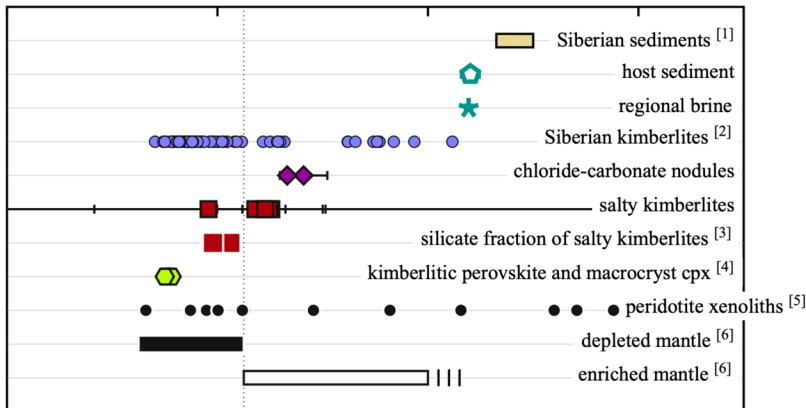
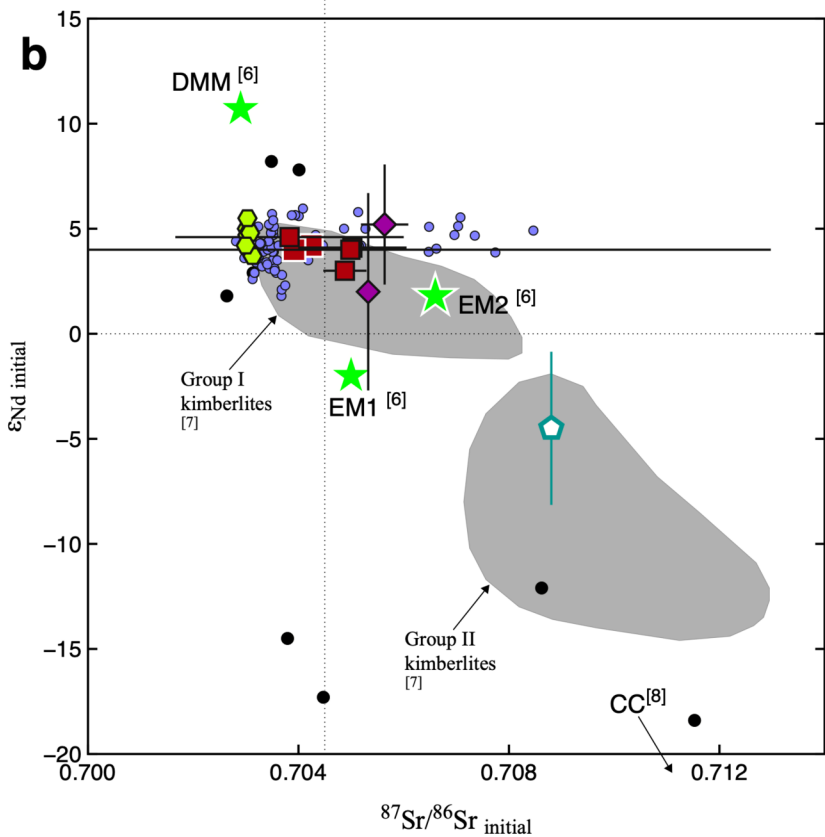
**Mineral compositions:**

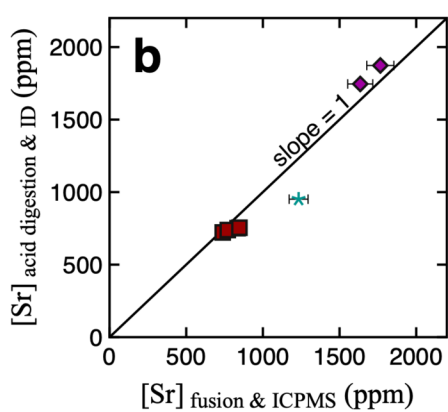
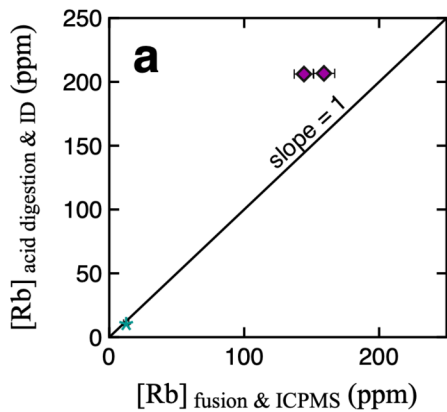
- olivine <sup>[1]</sup>
- ◆ alkali-carbonate sheets <sup>[2]</sup>
- chloride (halite to sylvite)
- mixing (sulfate - alkali-carbonate - chloride)
- ◆ carbonate (Sr-bearing calcite <sup>[3]</sup>, shortite <sup>[2]</sup> and sulfate (aphitalite <sup>[2]</sup>) compositions

**Whole-rock compositions:**

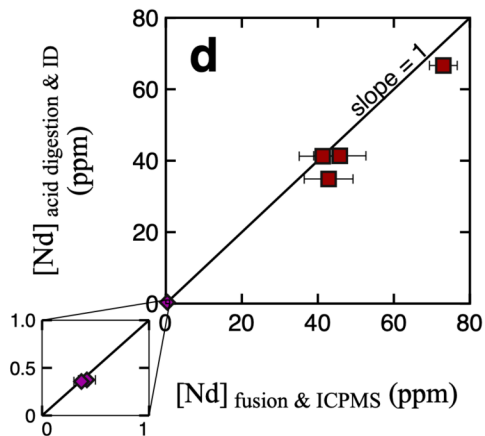
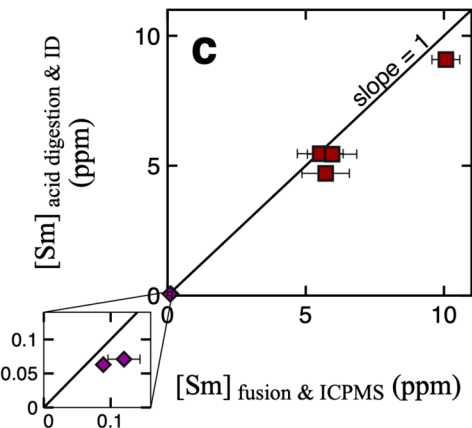
- ◆ chloride-carbonate nodule
- salty kimberlite <sup>[4]</sup>
- non-salty kimberlite <sup>[4]</sup>
- Siberian kimberlites <sup>[5]</sup>
- ▽ hydrothermal veins
- ★ brine precipitates
- ◇ host sediment



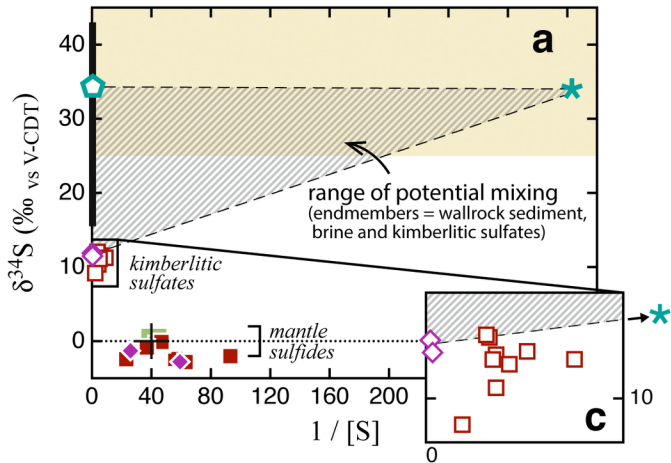
**a****b**



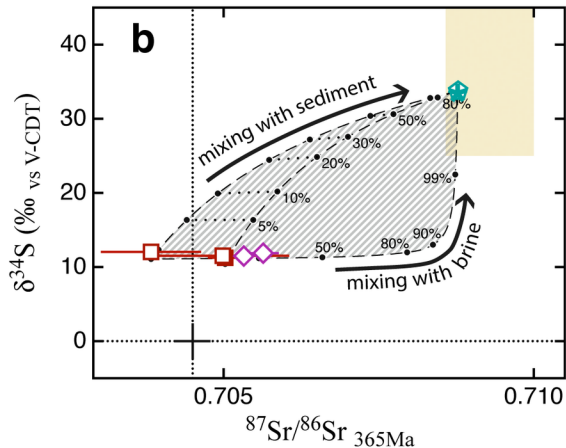
whole-rock:  
■ salty kimberlite  
◆ chloride-carbonate  
nodule  
\* regional brine



whole-rock:  
■ salty kimberlite  
◆ chloride-carbonate  
nodule



chloride-carbonate: ◆ sulfide ◇ sulfate  
 salty kimberlite: ■ sulfide <sup>[1]</sup> □ sulfate <sup>[1]</sup>  
 mantle range: ■ MORB <sup>[2]</sup> and peridotitic sulfides <sup>[3]</sup>  
+ primitive mantle <sup>[4]</sup>



sedimentary cover: ■ Siberian sediments & brines <sup>[5]</sup>  
⬠ wallrock sediment  
✱ regional brine  
 hydrothermal veins: — sulfates and sulfides <sup>[1]</sup>

mixing line and range

sample / salty kimberlite

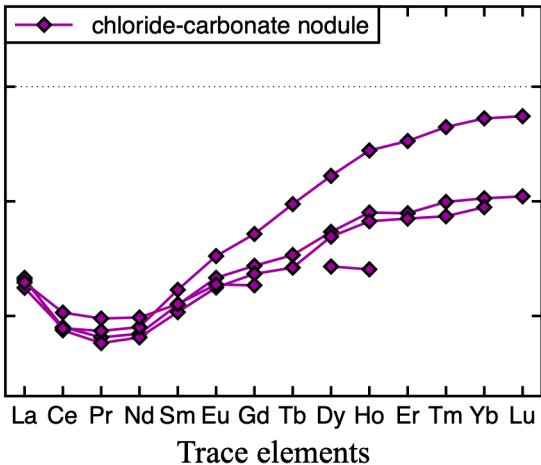


**Table 1:** Chloride fraction (in wt.%) estimated from major element compositions compared to weighed proportions (in wt.%) of the water leachates, acid leachates and residual solids of the leached samples.

<b>Sample</b>	<b>Rock type</b>	<b>estimated chloride fraction</b> <sup>[1]</sup>	<b>water leachate</b> <sup>[2]</sup>	<b>acetic acid leachate</b> <sup>[2]</sup>	<b>solid residue</b> <sup>[2]</sup>
UV11-201	chloride-carbonate nodule	28%	71%	26%	3%
UV11-203	chloride-carbonate nodule	34%	73%	26%	1%
UV09-305	host sediment	1%	5%	71%	24%

**Notes:**

[1] Percentage in the sample estimated from the major element composition of bulk powder assuming all Na and Cl form NaCl or KCl.

[2] Percentage in the sample estimated as the difference in weight before and after each leaching step.

**Table 2:** Major element compositions of salty kimberlites and chloride-carbonate nodules from the Udachnaya-East pipe, as well as hydrothermal veins from the same pipe and salt-bearing samples from the sedimentary cover.

Sample:	salty kimberlites				Chloride-carbonate nodules <sup>[1]</sup>				Hydrothermal salt veins <sup>[1]</sup>			Sedimentary cover <sup>[1]</sup>		
	UV04-24	UV11-70	UV12-119	UV12-120	UV11-180	UV11-201	UV11-203	UV11-203 picked carbonate	UV14-111 grey halite	UV14-111 colorless clear halite	UV14-111 clear blue halite	UV09-720 brine precipitate	UV14-brine regional brine [5]	UV09-305 host sediment
<b>Note:</b>														
<b>Major element compositions in oxide wt. %</b>														
SiO <sub>2</sub>	26.3	25.8	30.9	26.1	0.3	2.39	0.69	1.06	0.12	< L.D.	< L.D.	0.08	na	1.76
TiO <sub>2</sub>	1.56	1.24	1.23	1.05	< L.D.	< L.D.	< L.D.	< L.D.	< L.D.	< L.D.	< L.D.	< L.D.	na	< L.D.
Al <sub>2</sub> O <sub>3</sub>	2.08	1.55	4.36	1.60	< L.D.	0.37	0.12	0.295	< L.D.	< L.D.	< L.D.	< L.D.	na	0.11
FeO total	9.23	7.32	6.40	7.21	0.079	0.300	0.089	0.063	< L.D.	< L.D.	< L.D.	< L.D.	na	0.259
MnO	0.191	0.133	0.105	0.135	0.0023	0.017	0.0049	0.0044	0.0008	< L.D.	< L.D.	0.0045	na	0.02
MgO	31.2	28.8	22.3	29.4	0.256	1.54	0.44	0.638	0.071	< L.D.	< L.D.	0.191	na	15.5
CaO	11.0	9.9	10.8	11.7	10.0	13.5	14.1	17.8	0.523	< L.D.	< L.D.	0.75	na	29.3
Na <sub>2</sub> O	4.84	7.02	6.18	5.61	30.6	24.3	26.7	24.2	51.6	53.1	52.2	48.9	na	0.08
K <sub>2</sub> O	1.23	2.14	3.72	1.96	12.8	13.2	11.2	10.3	0.331	0.178	0.178	0.303	na	0.046
P <sub>2</sub> O <sub>5</sub>	0.73	0.39	0.47	0.41	< L.D.	0.14	0.17	0.23	< L.D.	< L.D.	< L.D.	< L.D.	na	< L.D.
LOI	11.6	20.2	14.4	18.2	nd	nd	nd	nd	nd	nd	nd	nd	na	40.9
Total <sup>[2]</sup>	100.0	104.5	100.9	103.3	54.1	55.8	53.5	54.5	52.7	53.3	52.4	50.2	na	87.9
CO <sub>2</sub> total	8.46	7.83	8.7	9.65	nd	17.2	19.2	24.9	0.39	0.11	0.1	0.04	nd	34.5
H <sub>2</sub> O+ total	0.27	0.56	0.18	0.38	nd	nd	nd	nd	nd	nd	nd	nd	na	nd
<b>Major element compositions in atomic wt. %</b>														
Si	12.3	12.0	14.4	12.2	0.14	1.12	0.32	0.50	0.06	< L.D.	< L.D.	0.04	< L.D.	0.82
Ti	0.94	0.74	0.74	0.63	< L.D.	< L.D.	< L.D.	< L.D.	< L.D.	< L.D.	< L.D.	< L.D.	< L.D.	< L.D.
Al	1.10	0.82	2.31	0.85	< L.D.	0.20	0.06	0.16	< L.D.	< L.D.	< L.D.	< L.D.	0.0007	0.06
Fe	7.17	5.69	4.98	5.61	0.06	0.23	0.07	0.05	< L.D.	< L.D.	< L.D.	< L.D.	< L.D.	0.20
Mn	0.15	0.10	0.08	0.10	0.00	0.01	0.00	0.00	< L.D.	< L.D.	< L.D.	< L.D.	0.005	0.01
Mg	18.8	17.4	13.5	17.7	0.15	0.93	0.26	0.38	0.04	< L.D.	< L.D.	0.12	9.1	9.32
Ca	7.88	7.11	7.74	8.38	7.17	9.66	10.1	12.7	0.37	< L.D.	< L.D.	0.54	52.1	20.9
Na	3.59	5.21	4.59	4.16	22.7	18.0	19.8	17.9	38.3	39.4	38.7	36.3	28.4	0.06
K	1.02	1.78	3.09	1.62	10.6	11.0	9.27	8.51	0.27	0.15	0.15	0.25	9.4	0.04
P	0.32	0.17	0.21	0.18	< L.D.	0.06	0.07	0.10	< L.D.	< L.D.	< L.D.	< L.D.	< L.D.	< L.D.
O	35.1	33.3	34.9	33.7	13.2	14.6	13.5	14.1	na	na	na	na	na	15.6
S	0.29	0.30	0.57	0.25	1.33	4.47	2.90	3.63	0.21	0.04	0.06	0.11	0.02	1.70
Cl	1.05	6.59	4.52	4.79	30.8	16.9	20.4	8.76	57.8	58.3	58.3	56.6	nd	0.35
Total <sup>[3]</sup>	98.5	99.6	100.5	100.2	86.3	94.3	96.0	91.7	97.5	98.0	97.3	94.0	99.0	83.6
K <sub>2</sub> O/Na <sub>2</sub> O	0.3	0.3	0.6	0.3	0.4	0.5	0.4	0.4	0.006	0.003	0.003	0.006	na	0.6
C.I. <sup>[4]</sup>	1.0	1.1	1.6	1.1	na	na	na	na	na	na	na	na	na	na

**Notes:**

[1] For salt analyses, LOI was not measured and [Cl], [CO<sub>2</sub>], and [S] were measured instead; [CO<sub>2</sub>] and [S] are considered qualitative given the salt matrix.

[2] Total oxide wt.% is the sum of major elements, using FeOtotal. When LOI was determined (e.g. kimberlite samples), total oxide wt.% is calculated using LOI and  $LOI \approx [Cl] + [CO_2] + [H_2O] + [S]$ . When LOI was not measured (e.g. salt-bearing samples), total oxide wt.% is calculated using  $[CO_2] + [H_2O]$  and is < 100% because [Cl] and [S] are not taken into account.

[3] Total atomic wt.% is the sum of major elements in atomic wt.%, plus [CO<sub>2</sub>] + [H<sub>2</sub>O]. Because it includes [S] and [Cl], it is usually  $\approx 100\%$ . Total atomic wt.% <100% indicate that either [CO<sub>2</sub>], [H<sub>2</sub>O], [Cl] or [S] was missing from the analysis.

[4] The contamination index of kimberlite samples is calculated such that  $C.I. = (SiO_2 + Al_2O_3 + Na_2O)/(MgO + 2*K_2O)$ , according to Kjarsgaard et al. (2009) and references therein. Although this index is not relevant for quantifying the contamination by surficial lithology (e.g. sediments), it gives an indication of the possible incorporation of continental granitic crust. Typically, C.I. values < 1 are considered uncontaminated.

[5] Concentrations in the brine solution are normalised to 100 atomic wt.% in order to allow for a direct comparison with rock samples. The measured total atomic wt.% was 12.51 wt.%, including both major and trace elements.

< L.D. is lower than detection limit; nd is not determined; na is not applicable.

**Table 3:** Trace element compositions of salty kimberlites and chloride-carbonate nodules from the Udachnaya-East pipe, as well as hydrothermal veins from the same pipe and salt-bearing samples from the sedimentary cover.

Sample:	salty kimberlites				Chloride-carbonate nodules				Hydrothermal salt veins			Sedimentary cover		
	UV04-24	UV11-70	UV12-119	UV12-120	UV11-180	UV11-201	UV11-203	UV11-203 picked carbonate	UV14-111 grey halite	UV14-111 colorless clear halite	UV14-111 clear blue halite	UV09-720 brine precipitate	UV14-brine regional brine [1]	UV09-305 host sediment
<b>Trace element compositions in ppm</b>														
As	1.9	< L.D.	< L.D.	< L.D.	< L.D.	3.4	3.1	3.2	< L.D.	< L.D.	< L.D.	< L.D.	< L.D.	< L.D.
Ba	966	896	1233	907	28	144	39	112	13	< L.D.	< L.D.	6.4	15	1162
Be	0.51	0.94	4.7	0.90	< L.D.	1.5	1.5	< L.D.	< L.D.	< L.D.	< L.D.	< L.D.	< L.D.	< L.D.
Bi	< L.D.	< L.D.	< L.D.	< L.D.	1.0	< L.D.	< L.D.	< L.D.	< L.D.	< L.D.	< L.D.	< L.D.	< L.D.	< L.D.
Cd	0.24	0.14	0.15	< L.D.	< L.D.	< L.D.	< L.D.	< L.D.	< L.D.	< L.D.	< L.D.	< L.D.	< L.D.	< L.D.
Ce	204	121	133	126	1.6	1.2	1.2	1.1	< L.D.	< L.D.	< L.D.	< L.D.	< L.D.	3.5
Co	80	73	62	75	< L.D.	3.5	1.5	< L.D.	< L.D.	< L.D.	< L.D.	< L.D.	0.61	0.85
Cr	1679	970	1131	924	35	28	29	15	90	76	86	76	< L.D.	4.7
Cs	0.40	0.28	1.8	0.38	0.60	0.93	1.2	0.84	< L.D.	< L.D.	< L.D.	< L.D.	2.6	< L.D.
Cu	74	55	61	46	24	10	< L.D.	< L.D.	< L.D.	< L.D.	< L.D.	< L.D.	7.6	< L.D.
Dy	3.3	1.8	1.8	1.8	0.061	0.38	0.12	0.11	< L.D.	< L.D.	< L.D.	< L.D.	< L.D.	0.24
Er	1.1	0.60	0.60	0.59	< L.D.	0.25	0.059	0.053	< L.D.	< L.D.	< L.D.	< L.D.	< L.D.	0.13
Eu	2.6	1.5	1.6	1.5	0.035	0.062	0.040	0.033	< L.D.	< L.D.	< L.D.	< L.D.	< L.D.	0.090
Ga	6.9	4.1	7.9	4.1	< L.D.	1.1	< L.D.	0.86	< L.D.	< L.D.	< L.D.	< L.D.	< L.D.	< L.D.
Gd	6.6	3.6	3.9	3.7	0.086	0.24	0.13	0.11	< L.D.	< L.D.	< L.D.	< L.D.	< L.D.	0.28
Ge	0.9	0.76	0.75	0.77	< L.D.	< L.D.	< L.D.	< L.D.	< L.D.	< L.D.	< L.D.	< L.D.	< L.D.	< L.D.
Hf	3.6	2.0	2.3	1.9	< L.D.	0.11	< L.D.	< L.D.	< L.D.	< L.D.	< L.D.	< L.D.	< L.D.	0.033
Ho	0.4	0.25	0.26	0.25	0.008	0.087	0.025	0.021	< L.D.	< L.D.	< L.D.	< L.D.	< L.D.	0.051
In	< L.D.	< L.D.	< L.D.	< L.D.	< L.D.	< L.D.	< L.D.	< L.D.	< L.D.	< L.D.	< L.D.	< L.D.	< L.D.	< L.D.
La	109	69	75	72	1.6	1.5	1.7	1.8	< L.D.	< L.D.	< L.D.	< L.D.	< L.D.	1.8
Lu	0.088	0.051	0.050	0.051	< L.D.	0.035	0.0070	< L.D.	< L.D.	< L.D.	< L.D.	< L.D.	< L.D.	0.018
Mo	1.3	2.8	3.0	1.6	10	24	25	20	< L.D.	< L.D.	< L.D.	< L.D.	< L.D.	< L.D.
Nb	174	110	112	105	0.68	0.41	0.30	< L.D.	< L.D.	< L.D.	< L.D.	< L.D.	< L.D.	0.20
Nd	73	41	46	43	0.51	0.42	0.37	0.34	< L.D.	< L.D.	< L.D.	< L.D.	< L.D.	1.7
Ni	1091	1120	851	1152	< L.D.	16	< L.D.	< L.D.	< L.D.	< L.D.	< L.D.	< L.D.	12	5.6
Pb	4.4	5.4	4.3	5.7	208	21	21	3.4	9.9	6.3	8.0	5.1	1.1	2.4
Pr	22	12	14	13	0.15	0.12	0.10	0.091	< L.D.	< L.D.	< L.D.	< L.D.	< L.D.	0.44
Rb	26	53	125	55	123	159	144	110	7.0	6.0	6.5	6.3	100	0.94
Sb	16	8.6	10	9.1	0.95	2.2	3.1	0.62	< L.D.	< L.D.	< L.D.	< L.D.	< L.D.	< L.D.
Sc	< L.D.	< L.D.	0.22	< L.D.	< L.D.	< L.D.	< L.D.	< L.D.	< L.D.	< L.D.	< L.D.	< L.D.	< L.D.	< L.D.
Sm	10	5.5	6.0	5.7	0.09	0.12	0.089	0.077	< L.D.	< L.D.	< L.D.	< L.D.	< L.D.	0.34
Sn	1.4	0.81	1.0	0.76	< L.D.	1.2	1.1	1.0	< L.D.	< L.D.	8.8	< L.D.	< L.D.	< L.D.
Sr	835	738	771	847	1313	1635	1766	2506	102	< L.D.	< L.D.	76	9863	51560
Ta	13	8.1	7.6	7.1	0.073	0.037	0.021	0.024	< L.D.	0.081	0.29	< L.D.	< L.D.	0.010
Tb	0.75	0.42	0.44	0.42	< L.D.	0.050	0.018	0.014	< L.D.	< L.D.	< L.D.	< L.D.	< L.D.	0.038
Th	15	8.4	9.4	8.9	< L.D.	< L.D.	< L.D.	< L.D.	< L.D.	< L.D.	< L.D.	< L.D.	< L.D.	0.079
Tm	0.11	0.066	0.066	0.064	< L.D.	0.036	0.0080	0.0060	< L.D.	< L.D.	< L.D.	< L.D.	< L.D.	0.017
U	2.3	2.1	2.3	2.1	< L.D.	0.079	0.087	< L.D.	< L.D.	< L.D.	< L.D.	< L.D.	0.020	0.56
V	97	94	126	89	37	72	64	74	29	28	28	25	< L.D.	1.7
W	0.83	1.5	1.9	1.7	7.0	22	17	18	< L.D.	< L.D.	< L.D.	< L.D.	< L.D.	< L.D.
Y	12	6.8	7.0	6.8	< L.D.	3.2	0.90	0.78	< L.D.	< L.D.	< L.D.	< L.D.	0.045	1.9
Yb	0.64	0.38	0.38	0.36	< L.D.	0.24	0.049	0.041	< L.D.	< L.D.	< L.D.	< L.D.	< L.D.	0.12
Zn	81	62	58	63	< L.D.	< L.D.	< L.D.	< L.D.	< L.D.	< L.D.	< L.D.	< L.D.	56	14
Zr	156	85	100	83	< L.D.	7.0	2.6	3.0	< L.D.	< L.D.	< L.D.	< L.D.	< L.D.	1.4

**Notes:**

[1] Concentrations in the brine solution are normalised to 100 atomic wt.% in order to allow for a direct comparison with rock samples. The measured total atomic wt.% was 12.51 wt.%, including both major and trace elements. Measured contents before normalisation were 13 ppm for Rb and 1233 ppm of Sr.  
< L.D. is lower than detection limit.

**Table 4:** Rb-Sr concentrations and isotopic compositions of salt-rich nodules and other samples from the Udachnaya-East kimberlite pipe and area.

Sample	Rock type	Method	Fraction	[Rb] (ppm)	± 2σ	[Sr] (ppm)	± 2σ	<sup>87</sup> Rb/ <sup>86</sup> Sr	± 2σ	<sup>87</sup> Sr/ <sup>86</sup> Sr	± 2σ	<sup>87</sup> Sr/ <sup>86</sup> Sr <sub>365Ma</sub> [4]	± 2σ
<b>UV11-201</b>	carbonate	[1]	whole-rock	206.64	1.10	1745.32	0.91	0.34	0.01	0.70739	0.00044	0.70564	0.00045
<b>UV11-203</b>	carbonate	[1]	whole-rock	206.12	1.16	1872.78	0.15	0.32	0.01	0.70695	0.00007	0.70532	0.00008
<b>UV04-24</b>	salty kimberlite	[2]	whole-rock	26.45	3.97	751.24	2.15	0.10	0.15	0.70435	0.00203	0.70383	0.00217
<b>UV11-70</b>	salty kimberlite	[2]	whole-rock	53.18	2.66	721.72	1.01	0.21	0.05	0.70611	0.00099	0.70502	0.00103
<b>UV12-119</b>	salty kimberlite	[2]	whole-rock	125.40	6.27	738.52	0.33	0.49	0.05	0.70739	0.00032	0.70488	0.00041
<b>UV12-120</b>	salty kimberlite	[2]	whole-rock	54.54	2.73	754.49	8.46	0.21	0.05	0.70606	0.00798	0.70499	0.00799
<b>UV09-305</b>	host sediment	[1]	leachate [3]	0.65	0.004	1878	0.47	0.001	0.01	0.70881	0.00018	0.70880	0.00018
<b>brine</b>	regional brine	na	solution	10.23	0.03	949.74	0.06	0.03	0.003	0.70893	0.00007	0.70877	0.00007

**Notes:**

[1] In this first method, we used acetic acid for the second leaching following water, and separated Rb and Sr using AG50-X8 cation resin.

[2] In this second method, we used HCl for the second leaching following water, and separated Rb and Sr using Sr-spec resin. For Sr-rich samples, columns with Sr-spec resin failed to separate Rb and Sr effectively enough to prevent some interference of <sup>87</sup>Sr on <sup>87</sup>Rb. The [Rb] and associated uncertainties for those samples correspond to SARM analyses.

[3] Due to the precipitation of fluorides when preparing the silicate residue of this sample, we only analysed its acetic acid leachate (71 wt.% of the whole-rock, Table 1).

[4] <sup>87</sup>Sr/<sup>86</sup>Sr ratios at the time of kimberlite eruption (365Ma) are calculated using the measured <sup>87</sup>Sr/<sup>86</sup>Sr and <sup>87</sup>Rb/<sup>86</sup>Sr ratios in the Rb-Sr decay equation:

$$^{87}\text{Sr}/^{86}\text{Sr} = [^{87}\text{Sr}/^{86}\text{Sr}]_{@365\text{Ma}} + ^{87}\text{Rb}/^{86}\text{Sr} * (e^{\lambda t} - 1)$$

where  $\lambda^{87}\text{Rb} = 1.3972 \times 10^{-11}$  per year is the decay constant of <sup>87</sup>Rb and  $t = 365 \times 10^6$  years is the time since eruption.

na: not applicable

**Table 5:** Sm-Nd concentrations and isotopic compositions of nodules and other samples from the Udachnaya-East kimberlite pipe and area.

Sample	Rock type	Fraction	[Sm] (ppm)	± 2σ	[Nd] (ppm)	± 2σ	<sup>147</sup> Sm/ <sup>144</sup> Nd	± 2σ	<sup>143</sup> Nd/ <sup>147</sup> Sm	± 2σ	εNd <sub>365Ma</sub> [2]	± 2σ
<b>UV11-201</b>	chloride-carbonate nodule	whole-rock	0.071	0.00001	0.374	0.0001	0.114	0.0003	0.512707	0.00015	5.21	2.86
<b>UV11-203</b>	chloride-carbonate nodule	whole-rock	0.063	0.00001	0.357	0.0002	0.107	0.0005	0.512525	0.00024	2.01	4.70
<b>UV04-24</b>	salty kimberlite	whole-rock	9.085	0.008	66.653	0.087	0.082	0.002	0.512600	0.00001	4.61	0.19
<b>UV11-70</b>	salty kimberlite	whole-rock	5.461	0.007	41.253	0.047	0.080	0.002	0.512570	0.00001	4.13	0.21
<b>UV12-119</b>	salty kimberlite	whole-rock	5.444	0.004	41.367	0.073	0.079	0.002	0.512514	0.00001	3.05	0.22
<b>UV12-120</b>	salty kimberlite	whole-rock	4.704	0.006	34.886	0.037	0.081	0.002	0.512569	0.00001	4.03	0.19
<b>UV09-305</b>	host sediment	leachate [1]	0.407	0.00007	2.186	0.001	0.112	0.0004	0.512206	0.00019	-4.50	3.64

**Notes:**

[1] Due to the precipitation of fluorides when preparing the silicate residue of this sample, we only analysed its acetic acid leachate (71 wt.% of the whole-rock, Table 1).

[2] <sup>143</sup>Nd/<sup>144</sup>Nd ratios at the time of kimberlite eruption (365Ma) are calculated using the measured <sup>143</sup>Nd/<sup>144</sup>Nd and <sup>147</sup>Sm/<sup>144</sup>Nd ratios in the Sm-Nd decay equation:

$$[^{143}\text{Nd}/^{144}\text{Nd}] = [^{143}\text{Nd}/^{144}\text{Nd}]_{@365\text{Ma}} + [^{147}\text{Sm}/^{144}\text{Nd}] \times (e^{\lambda t} - 1)$$

where  $\lambda^{147}\text{Sm} = 6.54 \times 10^{-12}$  per year is the decay constant of <sup>147</sup>Sm and  $t = 365 \times 10^6$  years is the time since eruption.

Nd isotopic compositions are then expressed in epsilon, as:  $\epsilon_{\text{Nd}} = (([^{143}\text{Nd}/^{144}\text{Nd}]_{\text{sample}} / [^{143}\text{Nd}/^{144}\text{Nd}]_{\text{CHUR}}) - 1) \times 10000$

where  $[^{143}\text{Nd}/^{144}\text{Nd}]_{\text{CHUR}} = 0.512170$  at 365 Ma, calculated from the current CHUR values of 0.512638 and a <sup>147</sup>Sm/<sup>144</sup>Nd ratio of the CHUR of 0.1967.

**Table 6:** S concentrations and isotopic compositions (as sulfide and sulfate) of nodules and other samples from the Udachnaya-East kimberlite and area

<b>Sample</b>	<b>Rock type</b>	$\delta^{34}\text{S}_{\text{sulfide}}$ (‰ vs V-CDT)	[S] <sub>sulfide</sub> (ppm)	$\delta^{34}\text{S}_{\text{sulfate}}$ (‰ vs V-CDT)	[S] <sub>sulfate</sub> (ppm)	$\delta^{34}\text{S}_{\text{bulk}}$ (‰ vs V-CDT)	[S] <sub>bulk</sub> (ppm)
<b>UV11-201</b>	chloride-carbonate	-1.24	386	11.86	38270	11.73	38656
<b>UV11-203</b>	chloride-carbonate	-2.72	169	11.47	25048	11.38	25217
<b>UV04-24</b>	salty kimberlite	-0.40	230	12.04	2724	11.07	2954
<b>UV11-70</b>	salty kimberlite	-2.82	159	11.25	2459	10.40	2618
<b>UV12-119</b>	salty kimberlite	nd	nd	11.40	2348	nd	> 2348
<b>UV12-120</b>	salty kimberlite	-2.40	178	11.51	1625	10.14	1803
<b>UV09-305</b>	host sediment	nd	nd	33.73	17000	33.73	17000
<b>UV14-brine</b>	brine	nd	nd	33.45	31	33.45	31

**Note:**

nd = not determined